November 3, 1984 SLAC proposal E140

A Proposal to Measure the x, Q^2 and Nuclear Dependence of $R = \sigma_L/\sigma_T$

The σ_L/σ_T Collaboration

R. Arnold, P. Bosted, G. deChambrier, S. Rock, Z. Szalata
The American University, Washington D. C. 20016

B. Filippone, R. McKeown, R. Milner, D. Potterveld
California Institute of Technology, Pasadena, CA 91125

A. Para
CERN, Genève, Switzerland

F. Dietrich, J. Woodworth
Lawerence Livermore National Laboratory, Livermore, CA 94550

B. Debebe, R. Hicks, G. Peterson
University of Massachusetts, Amherst, MA 01003

A. Bodek, T. Cormier, G. Gerbier,* K. Lang, P. Perez*
E. M. Riordan, M. Virchaux*
University of Rochester, Rochester, N. Y. 14627

O. Fackler
Rockefeller University, Rockefeller, N.Y. 10021

J. Alster, J. Lichtenstadt
University of Tel-Aviv, Ramat Aviv, Tel-Aviv 69978, Israel

R. Gearhart
Stanford Linear Accelerator Center, Stanford, CA 94305

Spokesmen: S. Rock (415-845-3300 x3454)
A. Bodek (716-275-3929)

* On leave from CEN Saclay. Participation by Saclay as an institution is pending approval by the Saclay program committee. At present these individuals are participating as visitors to Rochester University.

Summary

We propose to determine the ratio $R = \sigma_L/\sigma_T$ from deep inelastic electron-proton $(e-p)$, electron-deuteron $(e-d)$, electron-iron $(e-\mathrm{Fe})$ and electron-gold $(e-\mathrm{Au})$ scattering in the x, Q^2 range $0.1 \leq x \leq 0.5$ and $1 \leq Q^2 \leq 12.5\ (GeV/c)^2$. The absolute value of R as a function of x and Q^2 for hydrogen, deuterium, iron and gold will be measured with typical systematic errors of 0.035 and statistical errors of about 0.026. This will improve on existing SLAC data on hydrogen and deuterium that have typical systematic errors of 0.07 and statistical errors ranging from 0.07 to 0.15. The A-dependence of R and its relationship to nuclear effects, such as quark and gluon distributions in nuclei, will be investigated. The difference between R for heavy nuclear targets and R for the deuteron will be determined with a typical systematic error of 0.02. Incident electron energies will vary from 3 to 21 Gev with instantaneous currents ranging from 1 mA to maximum current through 0.4% slits. Beam from the full linac and from the new Nuclear Physics Injector will be used. We request 400 hours of running at 100% efficiency at 180 pps and three weeks of checkout and calibrations at low pulse rate.

Table of Contents

Figures

Tables

1. Introduction

The first crude determinations of the quantity $R = \sigma_L/\sigma_T$ in deep-inelastic electron scattering experiments had a significant impact on our understanding of nucleon structure. Early observations[1] that R was about 0.2 supported the idea that electrons were scattering from spin 1/2 constituents and provided evidence against early vector meson dominance models which predicted large values for R that increase with Q^2. Within the parton model, R is expected to be small for spin 1/2 constituents, while $R = \infty$ for spin 0 constituents. The second generation of deep inelastic experiments[2] at SLAC revealed a weak kinematic variation in R that was consistent with spin 1/2 partons, but could not rule out a small spin zero contribution.

During the last decade there have been significant theoretical advances in our understanding of inelastic scattering within the framework of Quantum Chromodynamics (QCD). Tests of these theoretical ideas require much better determinations of R than presently available. In addition, there are recent indications[3] that R may increase with atomic weight A. If such an A-dependence is confirmed, it would be difficult to understand within the present QCD framework, and may require additional concepts beyond our present quark-gluon picture of nucleons and nuclei in this region of dynamics.

In parallel with these theoretical advances, there have been marked improvements during the past few years in detector instrumentation, and the beam steering and intensity monitors in SLAC End Station A have been upgraded. These improvements, and further improvements that can be made, combined with a dedicated single spectrometer experiment, make better determinations of R experimentally feasible. As shown in the following sections, an improvement of a factor of at least 3 in statistical errors and 2 in systematic errors over previous SLAC experiments is possible.

Better determinations of R are also needed for accurate extraction of the structure functions F_1 and F_2 from cross sections measured in other experiments.

These structure functions, which are related to the quark distributions in nucleons and nuclei, are used in the study of scaling violations, and in the extraction of the strong coupling constant and the gluon distributions. Present uncertainties in R affect the accuracy of the structure function determination from measured deep inelastic cross sections. For example, an attempt by the European Muon Collaboration (EMC) to combine their high Q^2 muon scattering data on hydrogen[4] with the lower Q^2 data from SLAC[5] revealed a 10% difference in the region of overlap ($Q^2 = 10\ (GeV/c)^2$). The high energy muon data at this Q^2 are at small scattering angles, while the lower energy SLAC data are at large scattering angles, making the extraction of F_2 from these data sensitive to R. It was concluded[6] that if R were zero, the SLAC and EMC data would be consistent, and could be combined in a global study of scaling violations.

Evidence that the structure functions and therefore the quark and gluon distributions in heavy nuclei are different from those in deuterium (the EMC effect) was first obtained in muon scattering experiments[7] and subsequently observed[3,8] in electron scattering data from SLAC. This discovery had a significant impact on our views of the structure of nuclei, and has spurred the applications of the concepts of quarks, gluons and QCD to nuclear physics. A study of the nuclear dependence of R is needed for a thorough understanding of the origin of the EMC effect. At present, there is a difference at small x ($x < 0.2$) between the ratios of iron and deuterium cross sections as quoted by the EMC[7] and the same ratios as measured[3] at SLAC. A 0.15 difference in R between iron and deuterium (i.e. a factor of 2 change in R) would account for this difference,but no studies of $R_{Fe} - R_d$ exist in this region. There are indications of such a difference in the SLAC E139 data at $x = 0.5$, but it is only a 2 standard deviation effect.[3] No accurate studies of the nuclear dependence of R are presently available.

Finally, all present high statistics muon and neutrino data have been measured with nuclear targets, primarily iron.[9] A recent neutrino experiment,[10] although unable to determine R very well, has reported upper limits on the value

of R for iron at $x = 0.5$ and high Q^2 ($Q^2 = 50$ $(GeV/c)^2$). These limits can be combined with a Q^2 dependence study of R for iron at SLAC, where for $x = 0.5$, R can be determined over the range $2.5 < Q^2 < 12.5$ $(GeV/c)^2$ with good accuracy. Because the SLAC data will yield values for F_1 and F_2 separately, they can be combined with high Q^2 muon and neutrino data on iron in order to separate the higher twist and QCD contributions to scaling violations for one nuclear target. A discussion of all existing data on R is given in Section 4.

2. Kinematics for electron scattering

We describe the scattering of an electron of incident energy E from a nucleon (or nuclear target) to a final energy E' at a laboratory angle θ. In the first Born approximation, the scattering occurs through the exchange of a virtual photon of energy $\nu = E - E'$, and invariant four-momentum transfer $-q^2 = Q^2 = 4EE'\sin^2(\theta/2)$. The differential cross section is related to the structure functions W_1 and W_2 according to:

$$\frac{d^2\sigma}{d\Omega dE'}(E, E', \theta) = \sigma_M \Big[W_2(\nu, Q^2) + 2W_1(\nu, Q^2) \tan^2(\theta/2) \Big] \qquad (1)$$

where $\sigma_M = 4\alpha^2 E'^2 \cos^2(\theta/2)/Q^4$ is the Mott cross section.

We define all cross sections and structure function quantities for nuclear targets in terms of cross sections or structure functions *per nucleon*. Similarly, all kinematics are defined with respect to a stationary free proton target of mass M. Under such a definition, the Bjorken scaling variable $x = Q^2/2M\nu$ ranges from 0 to 1 for a proton target, and from 0 to M_A/M for nuclear targets where $M_A = AM$ is the mass of a nucleus of atomic weight A. The hadronic final state mass W, defined for the scattering from a free proton, is given by the expression $W^2 = M^2 + 2M\nu - Q^2$.

In the first Born approximation, the differential cross section can also be expressed in terms of total cross sections for the absorption of transverse and longitudinal virtual photons σ_L and σ_T:

$$\frac{d^2\sigma}{d\Omega dE'}(E,E',\theta) = \Gamma\Big[\sigma_T(\nu,Q^2) + \epsilon\,\sigma_L(\nu,Q^2)\Big] \tag{2}$$

where

$$\Gamma = \frac{\alpha}{4\pi^2}\frac{kE'}{Q^2E}\Big(\frac{2}{1-\epsilon}\Big), \tag{3}$$

$$k = \frac{W^2 - M^2}{2M}, \tag{4}$$

and

$$\epsilon = \Big[1 + 2(1+\frac{\nu^2}{Q^2})\tan^2(\theta/2)\Big]^{-1} \tag{5.a}$$

$$= \Big[1 + 2(1+\frac{Q^2}{4M^2x^2})\tan^2(\theta/2)\Big]^{-1} \tag{5.b}$$

The quantity Γ is the flux of transverse virtual photons and ϵ is the degree of longitudinal polarization. The cross sections σ_L and σ_T are related to the structure functions W_1 and W_2 by:

$$W_1(\nu,Q^2) = \frac{k}{4\pi^2\alpha}\sigma_T(\nu,Q^2) \tag{6.a}$$

$$W_2(\nu,Q^2) = \frac{k}{4\pi^2\alpha}\Big[\frac{Q^2}{Q^2+\nu^2}\Big]\Big[\sigma_T(\nu,Q^2) + \sigma_L(\nu,Q^2)\Big] \tag{6.b}$$

In the limit of $Q^2 \to 0$, the quantity $\epsilon \to 0$ and $\sigma_T \to \sigma_\gamma(\nu)$, where $\sigma_\gamma(\nu)$ is the photoproduction cross section for real photons. The quantity $R = \sigma_L/\sigma_T$ is related to the ratio of W_1 and W_2 by:

$$R(\nu,Q^2) = \frac{W_2}{W_1}(1+\frac{\nu^2}{Q^2}) - 1 \tag{7.a}$$

$$= \frac{F_2}{2xF_1}(1 + \frac{Q^2}{\nu^2}) - 1; \tag{7.b}$$

$$\text{or} \quad R(x,Q^2) = \frac{F_2}{2xF_1}(1 + \frac{4M^2x^2}{Q^2}) - 1 \tag{7.c}$$

where $F_2(x,Q^2) = \nu W_2(x,Q^2)$ and $F_1(x,Q^2) = MW_1(x,Q^2)$ are the structure functions which become functions solely of Bjorken x in the limit of exact scaling.

A separate determination of the inelastic structure functions F_1 and F_2 (or equivalently σ_L and σ_T) requires values of the differential cross sections at several values of the angle θ for fixed x and Q^2. This "Rosenbluth" separation requires taking data at different E and E' in order to keep x and Q^2 fixed as θ varies. According to Equation 2, σ_L is the slope and σ_T is the intercept of a linear fit versus ϵ of the quantity

$$\Sigma = \frac{1}{\Gamma}\frac{d^2\sigma}{d\Omega dE'}(x,Q^2,\epsilon) \tag{8.a}$$

$$= \sigma_T + \epsilon\sigma_L \tag{8.b}$$

The structure functions W_1 and W_2 (or F_1 and F_2) are then directly calculated from the extracted σ_L and σ_T using Equation 6. The relation between F_1, F_2, σ_L, and σ_T versus ϵ is shown schematically in Figure 1.

Alternatively, if we already *know* R, we can derive W_1 and W_2 from a single measurement of the differential cross section according to the following equations:

$$W_1 = \frac{1}{\sigma_M}\frac{d^2\sigma}{d\Omega dE'}\Big[(1+R)\Big(\frac{Q^2}{Q^2+\nu^2}\Big) + 2\tan^2(\theta/2)\Big]^{-1} \tag{9.a}$$

$$W_2 = \frac{1}{\sigma_M}\frac{d^2\sigma}{d\Omega dE'}\Big[1 + \Big(\frac{2}{1+R}\Big)\Big(\frac{Q^2+\nu^2}{Q^2}\Big)\tan^2(\theta/2)\Big]^{-1} \tag{9.b}$$

The measurements of R made in this experiment can determine functional forms for the kinematic variation of $R(x,Q^2)$ that can be used to separate the structure functions from the cross sections measured in other experiments.

$$\sum = \frac{1}{\Gamma}\frac{d^2\sigma}{d\Omega dE'}(x, Q^2, \varepsilon) = \sigma_T(x, Q^2) + \varepsilon \cdot \sigma_L(x, Q$$

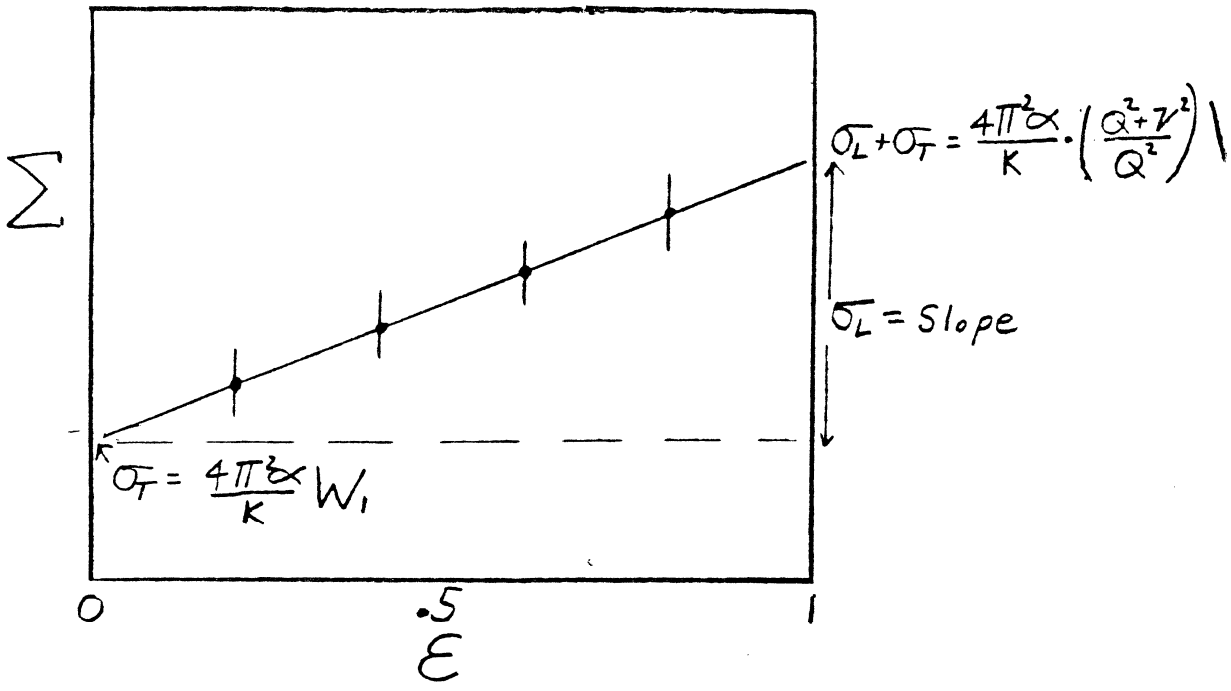

Figure 1. An example of the Rosenbluth separation of the longitudinal and transverse cross sections σ_L and σ_T. In the one photon exchange approximation, the cross section is a linear function of ϵ for fixed x and Q^2 (See Eq. 2).

Recently, it has become customary to express R in terms of the longitudinal structure function F_L and express the structure functions F_1 and F_2 in terms of quark and antiquark distributions in the nucleon (or nucleus).

$$\begin{aligned} R &= \sigma_L/\sigma_T \\ &= F_L/2xF_1, \end{aligned} \tag{10}$$

where

$$F_L = F_2 - 2xF_1 + \left(\frac{4M^2x^2}{Q^2}\right)F_2 \tag{11.a}$$

$$F_2 = (2xF_1 + F_L)\left[1 + \frac{4M^2x^2}{Q^2}\right]^{-1} \tag{11.b}$$

$$2xF_1(x,Q^2) = \sum_i e_i^2 q_i(x,Q^2) + \sum_j e_j^2 \bar{q}_j(x,Q^2) \tag{11.c}$$

Here $q_i(x,Q^2)$ and $\bar{q}_j(x,Q^2)$ are the probability for the quarks and antiquarks of charge e_i and e_j to carry a fraction x of the nucleon momentum.

High energy muon and neutrino cross sections can also be used to extract R using expressions analogous to Equations 1 and 2. These expressions are detailed in Appendix A, together with a discussion of the different assumptions involved. Suffice it to say here that cross section data must be measured for the same x, Q^2 at a wide range of energies and scattering angles if we wish to extract $R(x,Q^2)$. In neutrino scattering, R is extracted from the *sum* of neutrino and anti-neutrino cross sections.

3. Theory

The naive quark-parton model, neglecting target mass effects and finite transverse momenta, yields the Callan-Gross relation[11] $F_2 = 2xF_1$, or $R = Q^2/\nu^2 = 4M^2x^2/Q^2$, for scattering from massless spin 1/2 quarks. Note that this form implies that $R \rightarrow 0$ as $Q^2 \rightarrow \infty$ at fixed x, and satisfies the constraint $R = 0$ as $Q^2 \rightarrow 0$ required in the photoproduction limit where $\sigma_L(Q^2 = 0) = 0$. The inclusion[12] of finite transverse momenta p_t for the quarks in the naive quark-parton model yields the form

$$R_{naive} = \frac{4(M^2x^2 + < p_t^2 > \pm\Delta)}{Q^2 + < p_t^2 >}. \tag{12}$$

where finite mass effects are incorporated into Δ.

Current theoretical models consider the contributions to R from target mass effects, second order QCD, and possible higher twist terms. The finite p_t effects are generated by all three mechanisms. Target mass effects are included by using the Nachtman scaling variable ξ, where

$$\xi = \frac{2x}{1 + (1 + 4M^2x^2/Q^2)^{1/2}}. \tag{13}$$

This leads to values of R which are much smaller[13] than the values implied by $R = 4M^2x^2/Q^2$ (the naive Callan-Gross relation).

To first order, quantum chromodynamics does not add any contribution[13] to R, but second order QCD results in a contribution proportional to the strong coupling constant $\alpha_S(Q^2)$ that varies logarithmically with Q^2. This behavior can be understood as follows. Naively, finite transverse momenta add contibutions to R of order $4 < p_t^2 > /Q^2$, which fall like $1/Q^2$. In QCD, the quark effective transverse momentum is predicted to rise with Q^2 like $< p_t^2 >= \beta(x, Q^2)Q^2$ due to the exchange of virtual gluons. However, the coupling to the gluons in $\beta(x, Q^2)$ should fall like $1/\ln(Q^2/\Lambda^2)$ which yields

$$R_{QCD} \simeq \frac{r(x)Q^2}{Q^2 \ln(Q^2/\Lambda^2)}$$
$$\simeq \frac{r(x)}{\ln(Q^2/\Lambda^2)} \qquad (14)$$

where $r(x)$ is some function of x, which can have only a weak Q^2 dependence. The value of the longitudinal structure function is given by[14-18]

$$F_L^{QCD} = \frac{\alpha_s(Q^2)}{2\pi} x^2 \Big[\int_x^1 \frac{dz}{z^3} \frac{8}{3} F_2(z,Q^2) + \int_x^1 \frac{dz}{z^2} 2A(1-x/z) z g(z,Q^2) \Big] \qquad (15)$$

where $zg(z,Q^2)$ is the distribution of the gluons and $F_2(z,Q^2)$ is the distribution of the quarks in fractional momentum z. The constant A equals 20/9 for electroproduction and 8 for neutrino scattering. The strong coupling constant is given by $\alpha_S(Q^2) = 12\pi/(33-2n_f)\ln^{-1}(Q^2/\Lambda^2)$, where n_f is the number of flavors (3 to 4 for the Q^2 range at SLAC) and the QCD scale parameter Λ is of order 250 MeV.

The integrals in Equation 15 indicate that the longitudinal structure function will peak at small values of x and be small at large values of x. Note that the QCD expressions yield R_{QCD} which is the same for electron and neutrino scattering for an isoscalar target ($R_\nu^d = R_e^d$), because $R = F_L/2xF_1$ and $F_{1\nu}^d = (18/5)F_{1e}^d$. Another interesting consequence of Equation 15 is that if we assume that the gluon distributions are the same in the neutron and the proton, we find that the QCD contribution to R is about 20% larger for the neutron than for the proton. This happens because F_{1n}/F_{1p} is about 2/3 on the average and the gluon contributions to F_L in Equation 15 are the same for neutrons and protons. However, the absolute contribution to R from QCD effects is very small, especially at large x, and is of order 0.01 to 0.02 at $x = 0.5$. Calculations[19] to fourth order in QCD yield R values which are only slightly smaller that those

obtained from second order QCD due to a cancellation between the corrections to σ_L and σ_T. The CCFR collaboration has parametrized the QCD prediction[20,21] for R_{QCD} and obtains[22]

$$R^{Fe}_{QCD}(x,Q^2) \simeq \frac{0.73(1-x)^{3.7}}{\ln(Q^2/0.24^2)}. \tag{16}$$

This gives a value of 0.01 for R at $x = 0.5$ and $Q^2 = 10\ (GeV/c)^2$.

Aside from the target mass ξ scaling terms (which fall as $1/Q^2$) and the perturbative QCD contribution to R, which fall as $1/\ln(Q^2/\Lambda^2)$, there are possible higher twist contributions[23] that fall as a power series in $(1/Q^2)^n$. Under the simplest assumptions the higher twist contribution can be identified with the "intrinsic" transverse momentum contribution $R_{p_t} = 4 < p_t^2 > /Q^2$. It has been suggested that the transverse momenta of dimuon pairs produced in hadronic collisions should be identified with the intrinsic p_t of the partons. Such an assumption[24] leads to large values of R_{p_t} since the dimuon transverse momenta increase with the dimuon mass (which can be identified with Q^2). However, this transverse momentum cannot be directly plugged into the R_{p_t} expressions.[25] A detailed QCD analysis[26] of dimuon production indicates that the large transverse momenta of dimuon pairs, as well as the transverse momenta of high p_t hadronic jets[27] originate primarily from hard gluon radiation, which is already included in the calculations of R_{QCD}. The remaining "intrinsic" transverse momentum $< p_t^2 >$ is about[26] $0.04\ (GeV/c)^2$ at $x = 0.5$, becoming much smaller near $x = 0$ and $x = 1$. Therefore, if we take this intrinsic p_t we obtain that $R_{p_t} < 0.16/Q^2$ at $x = 0.5$ and it decreases to zero near $x = 0$ and $x = 1$. Another analysis[28] obtains even smaller values of intrinsic $< p_t^2 >$.

Higher twist effects in the form of diquark states[29,30] have also been suggested to give an increase in R at SLAC values of Q^2. Diquark models in general do not have much *a priori* predictive power.[25] There are severe disagreements among the various models[30,31,32] as to how diquarks interact with neutrinos. Early diquark models[29] which were proposed to explain large values of R in

the SLAC energy range[37,38] have difficulty with muon and neutrino data which became available recently. These include the neutrino measurements on the ratio of d/u quark distributions in the nucleon,[33,34] and the muon measurements[35] of the ratio F_{2n}/F_{2p} in the high Q^2 region. The SLAC data[5] on F_{2n}/F_{2p} agree with the muon data as well as with the predicted ratio based on the measured d/u quark distributions. Diquark models require a large variation with Q^2 of the F_{2n}/F_{2p} ratio, in disagreement with what has been observed at SLAC.

A study of the x, Q^2 dependence of R is a good test of QCD predictions, since QCD theories, including ξ scaling, make definite predictions for R — that R is small at large x. Higher twist effects should fall with Q^2. The QCD perturbative contributions can be calculated given the present knowledge of the scale parameter Λ and the gluon distributions. A large increase of R with nuclear weight cannot be accomodated within QCD, and should also serve as a good test of the theory. Therefore, a study of the nuclear dependence of R will test the quark-gluon picture of nuclei. This is especially true at large x (near $x = 0.5$) where the perturbative QCD calculations indicate that R should be very small. A study of the nuclear dependence of R at small values of x should help clarify the present disagreement between the SLAC and EMC data about the nature of the EMC effect at small x.

4. Comparisons of present data and theory

Average Values of R_p and R_d: Determinations of R in the deep inelastic region and SLAC energy range have typically been byproducts of experiments which were designed to concentrate on other aspects of structure function physics (e.g. F_{2n}/F_{2p}, $F_2(x, Q^2)$, A-dependence). Therefore, extensive interpolations of cross sections were needed to obtain data at fixed x and Q^2. Similary, since one experiment did not typically have a sufficient range in ϵ (or equivalently in angle) most R extractions have relied on combination of data sets measured at different times, with different targets, and with different End Station A spectrometers.

The full ϵ range actually available was not used and the separations relied on whatever ϵ range happened to be measured. An analysis of SLAC experiments E49B[2] and E87[5] (both using the 8 GeV/c spectrometer, but done at different times using different targets), and augmented with data taken in SLAC experiment E49A (taken with the 20 GeV/c spectrometer) was performed by the MIT-SLAC-SFG group (MIT-SFG)[5] . An analysis performed[37,38] by SLAC Group A utilized data from SLAC experiment E89 using both the 1.6 GeV/c and the 20 GeV/c spectrometers. In addition, SLAC Group A has performed a combined analysis[37,38] using the E89 data in combination with the E49B/E87 SLAC-SFG data. Table I summarizes the average values of R_p and R_d obtained from various analyses of SLAC data.

The MIT-SFG average values for R averaged over x and Q^2 in the range $0.1 \leq x \leq 0.8$ and $1.0 \leq Q^2 \leq 16$ $(GeV/c)^2$ are $R_p = 0.138 \pm 0.011 \pm 0.056$, and $R_d = 0.175 \pm 0.009 \pm 0.060$, where the second error is the overall systematic error. A restricted analysis using the data from only one spectrometer, but from different experiments and targets (E49B/E87), yields the average values $R_p = 0.136 \pm 0.017$ and $R_d = 0.137 \pm 0.013$ with similar systematic errors. Although in principle using data from one spectrometer should result in smaller systematic errors, this is only true if data over a large range of ϵ happen to be available (which was not the case here), and if the measurements were done at the same time. The systematic errors on the individual MIT-SFG values of R at different (x, Q^2) points are typically 0.07 but vary from 0.027 to 0.229, depending on the ϵ range that was available and on the data sets used. For $x > 0.2$ the error in the radiative correction is only a small part of the systematic error. Normalization factors were applied to account for overall differences between the various data sets. Typically 1-2% corrections, these factors were obtained either by a comparison of elastic cross sections (E49A/E49B) or by a comparison of inelastic cross sections taken at identical kinematic points (E49B/E87).

In the SLAC Group A analysis,[37,38] possible normalization differences were only incorporated into the systematic errors. These data, using the 20 GeV/c and

Table I

Average values of R_p and R_d and the difference $\delta = R_d - R_p$ from various analyses of SLAC data. Where two errors are shown, the first is the statistical error and the second is the systematic error.

Group	Experiments	Spectrometers	$< R >$
MIT-SLAC	E4	8/20	$R_p = 0.18 \pm 0.10$ (total)
MIT-SFG	E49/E87	8/20	$R_p = 0.138 \pm 0.011 \pm 0.056$ $R_d = 0.175 \pm 0.009 \pm 0.060$ $\delta = 0.031 \pm 0.015 \pm 0.036$
MIT-SFG	E49B/E87	8	$R_p = 0.136 \pm 0.017 \pm 0.06$ $R_d = 0.137 \pm 0.013 \pm 0.06$ $\delta = 0.02 \pm 0.03$ (total)
SLAC-GrpA	E89	1.6/20	$R_p = 0.30 \pm 0.10$ (total)
SLAC-GrpA	E49/E87/E89	1.6/8/20	$R_p = 0.21 \pm 0.10$ (total) $R_d = 0.22 \pm 0.10$ (total)

the 1.6 GeV/c spectrometer (E89) yield an average value of $R_p = 0.30 \pm 0.10$ where the error includes both statistical and systematic errors. An anlysis combining all available data (including the MIT-SFG data sets) yields $R_p = 0.21 \pm 0.10$ (total error). The problem of normalization between data sets apparently dominates the systematic errors; a single experiment using a single spectrometer over a wide range of ϵ can reduce the errors substantially.

R_p Versus x Averaged Over Q^2: Although interesting, the average value of R_p is not very informative since variations in both x and Q^2 are expected theoretically, and the average value should therefore depend on the x and Q^2 ranges of the various experiments. We next show the R data averaged over only Q^2. Figures 2 and 3 show R_p averaged over Q^2 for fixed values of x. The MIT-SFG data[5] and the Group A E89 data[28] are shown in Figure 2, along with theoretical contribution to R_p from target mass effects[12] in the SLAC average Q^2 range (dashed line), and from QCD terms[29] (solid line). Figure 3 shows the results of Group A's combined analysis[27,28] of all SLAC experiments. The errors shown include both statistical and systematic errors. The Group A values of R are uniformily higher than the MIT-SFG data, and *both* are high relative to theoretical predictions.

R_p Versus x and Q^2: We next look at R versus both x and Q^2. Detailed QCD analysis also including target mass corrections has been done by De Rujula et al[16] and by Buras et al.[18] A comparison of the De Rujula et al predictions with the MIT-SFG and SLAC E89 data is shown in Figure 4. The Buras et al prediction is similar. These 1977 predictions overestimate R_p by 0.01 to 0.02 because large values of Λ ($\Lambda = 500\ MeV$) and hard gluon distributions were used in the calculations. The present SLAC data are consistent with QCD predictions at low x and seem relatively higher at $x > 0.5$, but the statistical and systematic errors in R are too large to make any firm conclusions. Much more stringent tests of QCD can be made with the more accurate R data that can be measured at SLAC. If values of R of about 0.3 were to be determined with small error bars

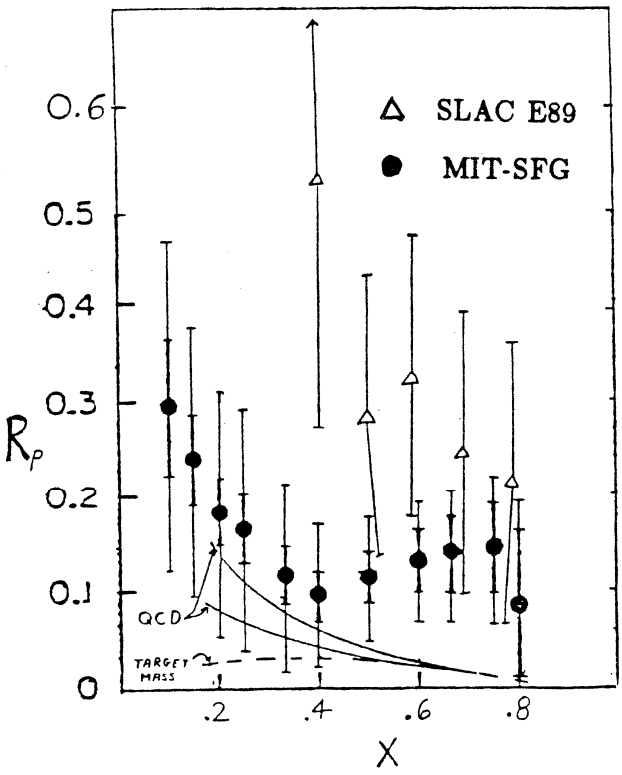

Figure 2. SLAC data for R_p averaged over Q^2 for bins in x. The statistical (inner) and systematic (outer) errors are shown for the MIT-SLAC data (Ref. 5). The combined error is shown for the Group A E89 data (Refs. 37,38). The dashed line is the expected contribution of target mass effects from R. Barbieri et al (Ref. 13). The solid lines are the expected QCD effects from Abbott et al (Ref. 29) for values of Q^2 in the range of the data.

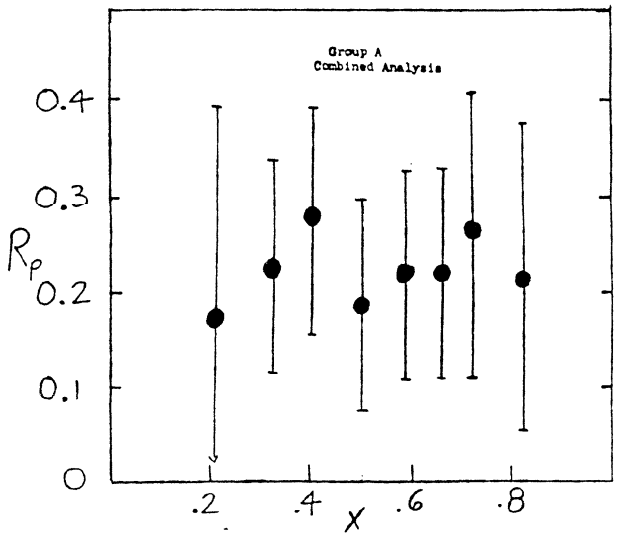

Figure 3. The combined MIT-SFG and SLAC Group A E89 data from an analysis by Mestayer et al (Refs. 37,38). The errors include both statistical and systematic errors.

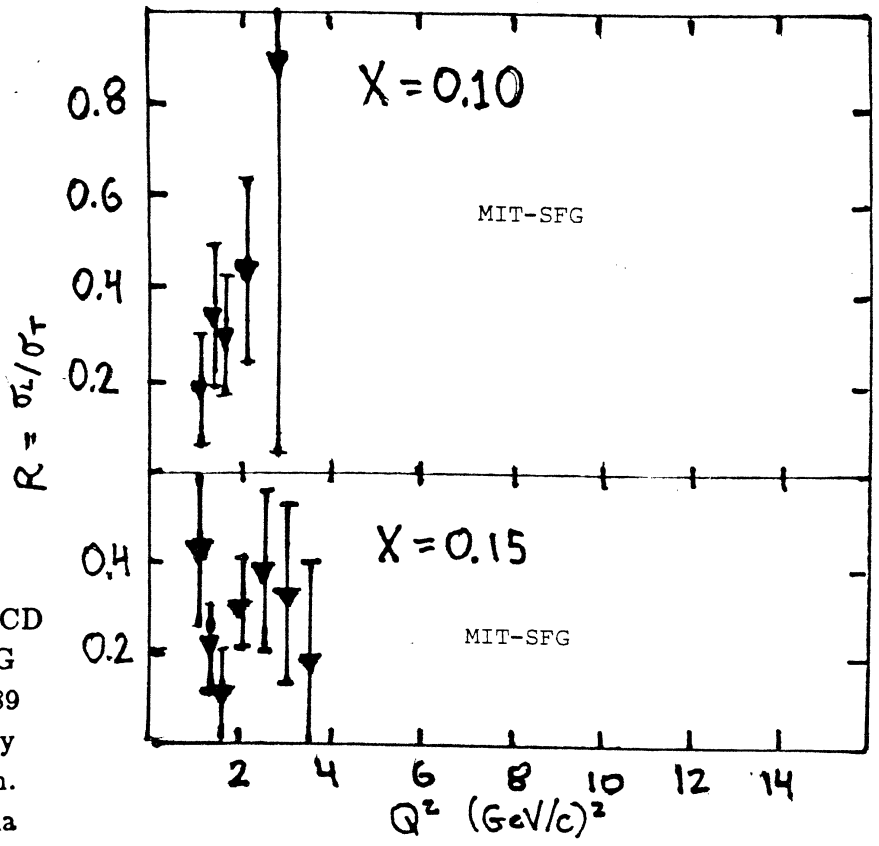

Figure 4. Comparison of QCD predictions with MIT-SFG data (Ref. 5) and SLAC E89 data (Refs. 37,38). Only statistical errors are shown. The solid line by DeRujula et al (Ref. 16) contains the sum of contributions from QCD and target mass effects. This figure continued on the next page.

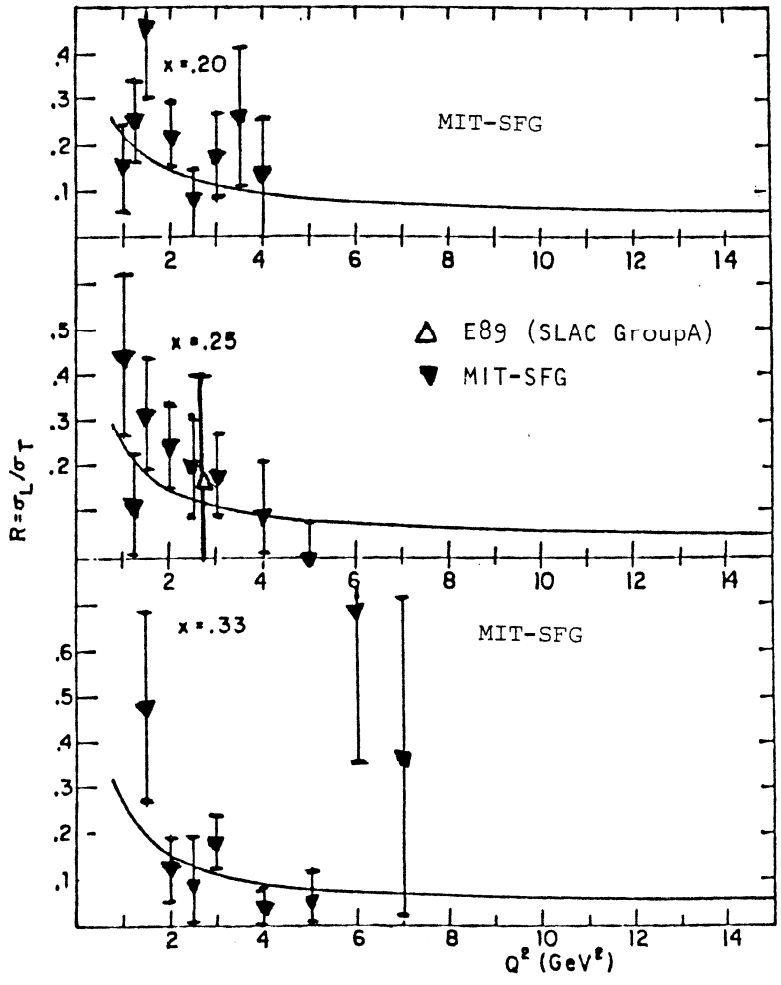

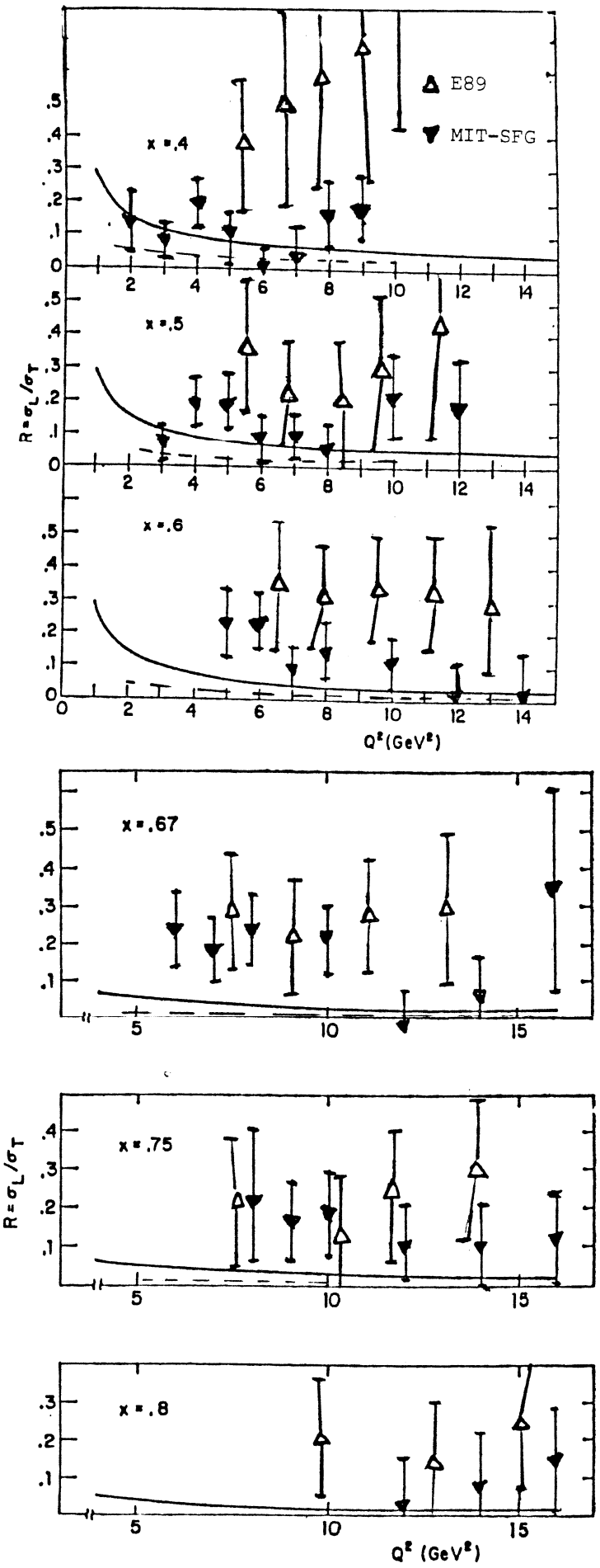

Figure 4 continued. Comparison of theoretical predictions with the MIT-SFG and SLAC E89 data. The solid line is the sum of contributions from QCD and from target mass effects from DeRujula et al (Ref. 16). The dashed line from Buras et al (Ref. 18). is a QCD prediction without target mass terms, but otherwise similar to the DeRujula et al calculation.

at $x = 0.5$ and $Q^2 = 10\ (GeV/c)^2$ for *any* target (hydrogen, deuterium, or iron) it would present a challenge to the theory. It would be even more challenging to the theory if we confirm that R is independent of Q^2 over the SLAC energy range as suggested, though with large errors, by the combined analysis of SLAC Group A.

The only other existing data on R for a hydrogen target come from muon scattering experiments at Fermilab[39] (CHIO) and at CERN[40] (EMC). Such results are obtained from data taken at three different energies at three different times. The CHIO experiment took data with 96, 147 and 219 GeV muons and reports an average value of R_p of 0.52 ± 0.35 (total error) in the region $0.003 < x < 0.1$ and $0.4 < Q^2 < 30\ (GeV/c)^2$. These data averaged over Q^2 for various x bins are shown in Figure 5.

The EMC collaboration extract values for R_p from data taken with 120, 200 and 280 GeV muons.[40] They obtain an average value of $R_p = 0.00 \pm 0.10$ (total error) or $0.10 \pm 0.035 \pm 0.095$ (the second error is a systematic error) for the range $0.04 < x < 0.30$ and $5 < Q^2 < 145\ (GeV/c)^2$. The mean Q^2 is quoted as 22.5 $(GeV/c)^2$ and the mean ν 100 GeV. The EMC data, averaged over Q^2 for various x bins, are shown in Figure 6. Also shown is the curve expected from a QCD calculation as a function of x for the mean Q^2 of the EMC data. It appears that the CHIO muon experiment obtains an average R_p which is larger than the values expected from QCD at small x and the EMC obtains an average value which is smaller. The statistical and systematic errors are large, so no contradiction with QCD, or between the two experiments can be claimed.

The above results are indicative of what has been obtained from *all* the muon data runs over the last ten years. The results suffer from poor statistics and large systematic errors. Systematic errors arise from the fact that data can be taken only at a few energies (given a finite amount of time) since a run at each energy takes many months. Measurements of R at large values of x are not possible, nor can muon experiments achieve statistics sufficient to study both x and Q^2

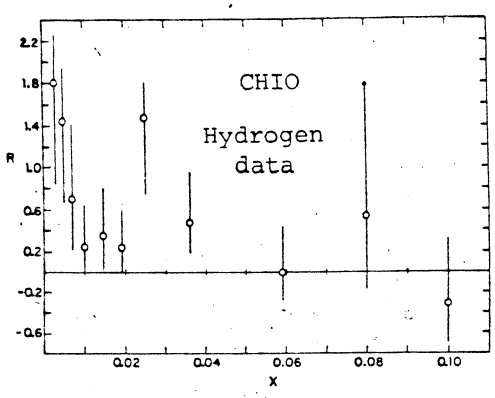

Extracted values of R vs x using the data-comparison technique. The average value of Q^2 for each point is different, and decreases with x.

Figure 5. The CHIO muon data on R for Hydrogen (Ref. 39).

Figure 6. The EMC data on R for hydrogen, averaged over Q^2 The data and curves are from Ref. 40.

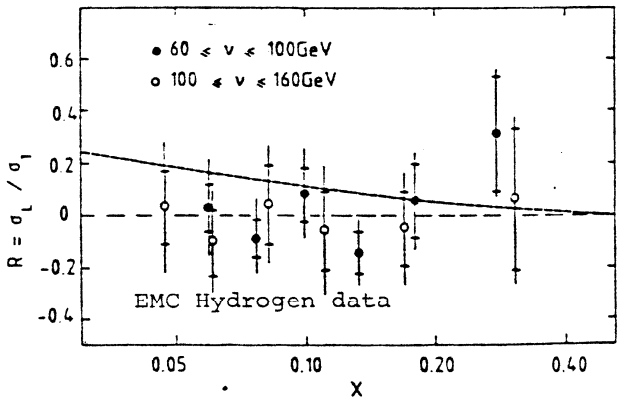

R as a function of the Bjorken variable x. Statistical errors are given separately by the inner bars. Dashed line: leading order QCD prediction

dependences of R. The only other muon data expected in the future will come from the muon program at the Tevatron.[36] The statistical precision is not expected to be improved over that of existing data (although higher Q^2 data will be available given the higher energies at the Tevatron). Therefore, no better determinations of R are expected from future muon experiments.

R_d Versus x Averaged Over Q^2: The only determinations of R for deuterium are from SLAC experiments. Data from MIT-SFG and experiment E139 are shown in Figure 7. SLAC experiment E139 quotes[8] an average value of $R_d = 0.112 \pm 0.048$ (statistical error) for $Q^2 = 5$ $(GeV/c)^2$ and averaged over $x = 0.3$, $x = 0.5$, and $x = 0.7$ points. These data are in agreement with the value of 0.18 ± 0.03 which is the average of the MIT-SFG data[5] at $x = 0.5$. Average values of R_d over the entire SLAC kinematic range (See Table I.) have been obtained by the MIT-SFG group[5] ($R_d = 0.175 \pm 0.009 \pm 0.060$) and by the combined analysis of SLAC Group A[37,38] ($R_d = 0.22 \pm 0.10$).

The Difference $R_d - R_p$: A more detailed comparison of R_d and R_p (which also holds for any comparison of R for two different targets) can be achieved[2,5] by extracting the quantity $\delta = R_d - R_p$ from the ratio of differential cross sections σ_d/σ_p in a method that exploits the small systematic uncertainty in this ratio. We obtain

$$\frac{\sigma_d}{\sigma_p} = \frac{\sigma_{Td} + \epsilon\sigma_{Ld}}{\sigma_{Tp} + \epsilon\sigma_{Lp}} \tag{17.a}$$

$$= T\left(\frac{1 + \epsilon R_d}{1 + \epsilon R_p}\right) \tag{17.b}$$

$$= T(1 + \epsilon'\delta) \tag{17.c}$$

$$\approx T[1 + \epsilon(R_d - R_p)] \tag{17.d}$$

where $T = \sigma_{Td}/\sigma_{Tp}$ and $\epsilon' = \epsilon/(1 + \epsilon R_p)$. The physical meaning of Equation 17 is clear: a difference between R_p and R_d results in a slope in σ_d/σ_p plotted versus ϵ' (or essentially versus ϵ). This difference $\delta = R_d - R_p$ has been extracted by the

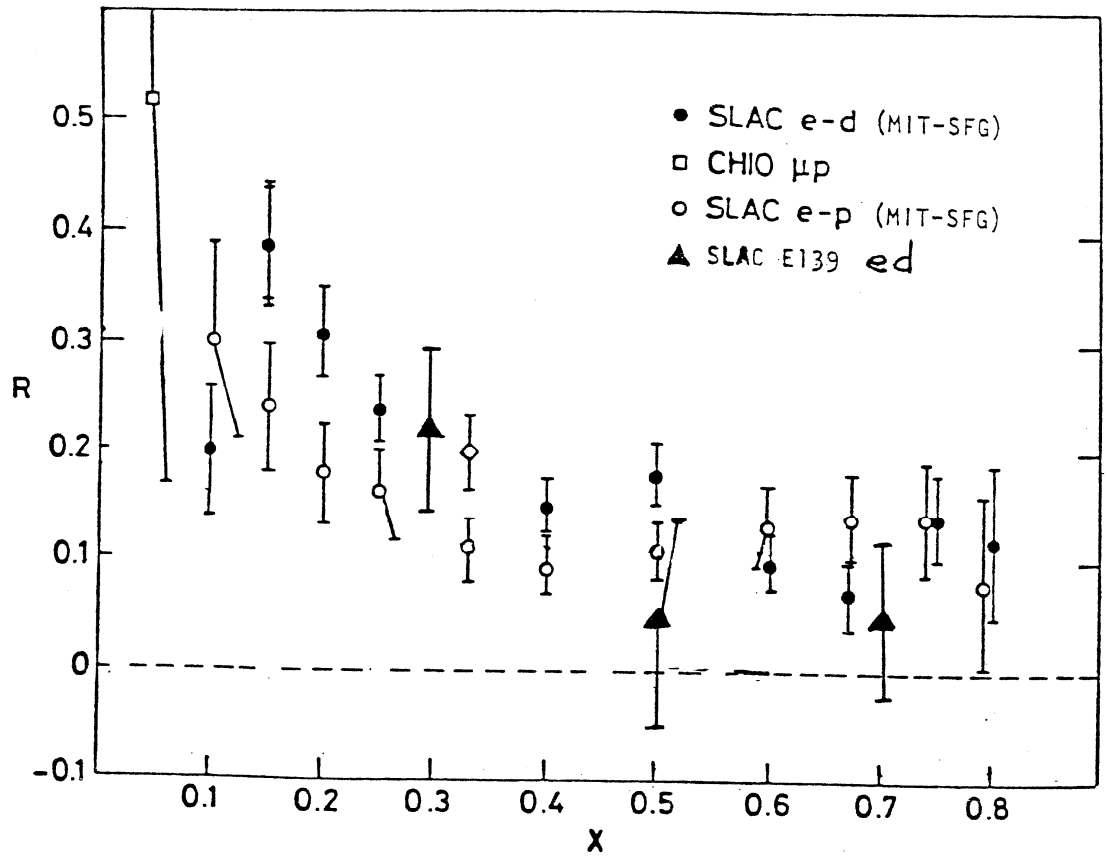

Figure 7. The MIT-SFG data (Ref. 5), averaged over Q^2 for hydrogen and deuterium. Also shown are the SLAC E139 deuterium data (Ref. 3) for $Q^2 = 5$ $(GeV/c)^2$

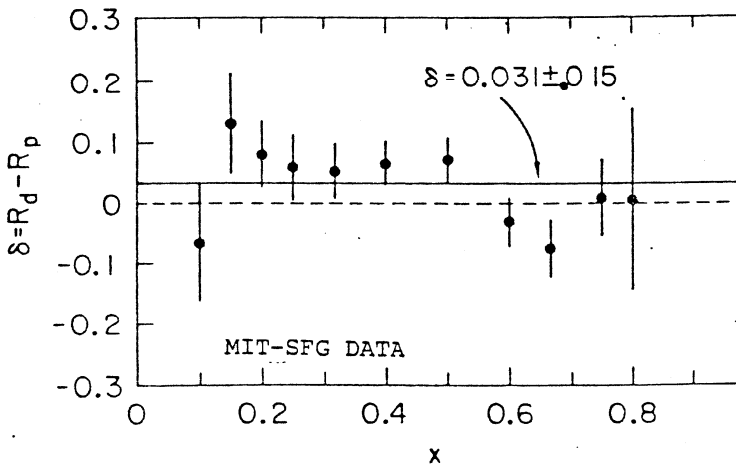

Figure 8. The difference between R_d and R_p averaged over Q^2 for bins in x from the MIT-SFG data (Ref. 5). Only statistical errors are shown. The systematic error is ± 0.036.

MIT-SFG group.[5] The data averaged over Q^2 for various bins in x are shown in Figure 8. The average value of δ is $< \delta >= 0.031 \pm 0.015 \pm 0.036$. Although this difference is consistent with zero given the systematic errors, the data are also consistent with a non zero value which is a function of x. A reduction in the systematic error by a factor of 2 (to ± 0.02) could reveal a significant difference between R_d and R_p. This difference could then be interpreted as a difference between R_p and R_n, which might be expected in QCD models.

R for Nuclear Targets: Finally we turn to a discussion of measurements of R on nuclear targets. At present all high statistics neutrino and muon experiments use heavy nuclear targets, and the determinations of R from such experiments are still not very good.[9] The CDHS collaboration has used neutrino data on iron taken with a narrow band neutrino beam.[10] They quote an average value of $< R_{Fe} >= 0.10 \pm 0.025 \pm 0.06$. They also use high statistics antineutrino data taken in a wide band beam to obtain limits on R at large x and large Q^2 (see Table II). Their results are shown in Figure 9, along with the predicted QCD values. Preliminary data from the CCFRR collaboration (MacFarlane thesis[22]), are compared with CDHS data on R_{Fe} is shown in Figure 10. The CHARM collaboration is the only group to have attempted to extract R from data taken with a wide band neutrino beam. They use a marble target[41] and obtain a mean value $< R >= 0.12 \pm 0.06$. Their data, averaged over Q^2 (statistical errors only) are shown in Figure 11. The CDHS collaboration, running in the same beam with a factor of 10 more data has not attempted such an extraction. It is an open question whether the neutrino flux in a narrow band beam is known to a sufficient accuracy to determine R_{Fe} with the systematic error of 0.06 as claimed, given the present disagreements among various neutrino experiments[10,22] on the determination of the neutrino cross sections. The systematic errors in a wide band beam are certainly much larger.

The European Muon Collaboration presented preliminary data on R_{Fe} at the Brighton conference.[42] A reanalysis of the hydrogen data yields an average

Table II

Upper limits for $R = \sigma_L/\sigma_T$ at large x

CDHS Iron data (neutrinos)

x	0.35	0.45	0.55	0.65
$R = \sigma_L/\sigma_T \leq$	0.152	0.058	0.022	0.017
σ_{stat}	0.019	0.019	0.024	0.033
σ_{syst}	0.042	0.022	0.025	0.035
$\langle Q^2 \rangle$ [GeV^2/c^2]	30.0	37.0	39.0	37.0

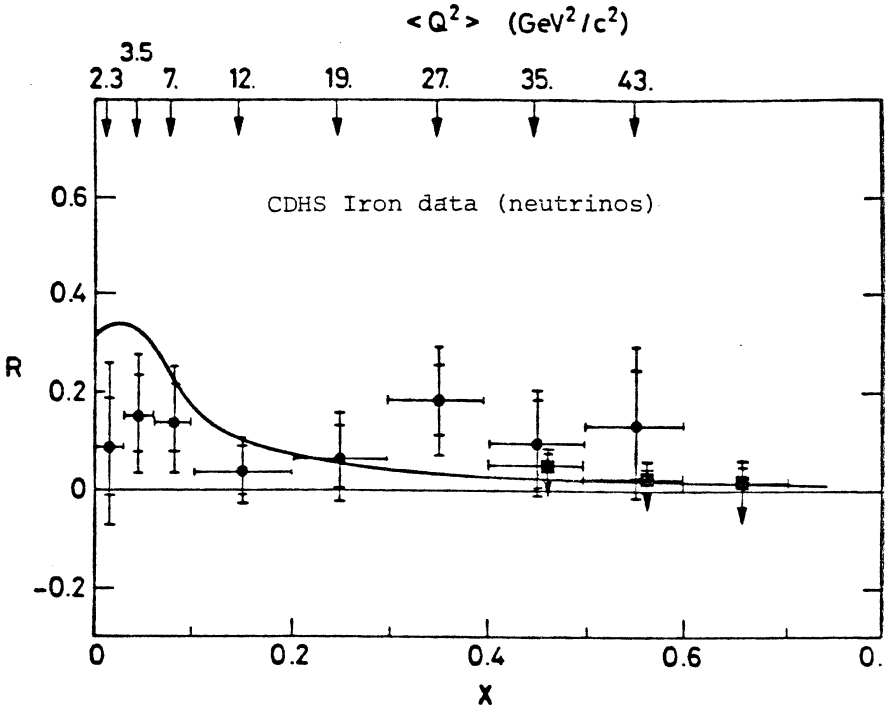

Figure 9. The CDHS narrow band data for R_{Fe} (Ref. 10). Data have been averaged over Q^2 for bins of x. Upper limits on R_{Fe} from wide band (horn) antineutrino data are shown in the figure and given in Table III. The curve is the expectation from QCD as calculated by the CDHS group.

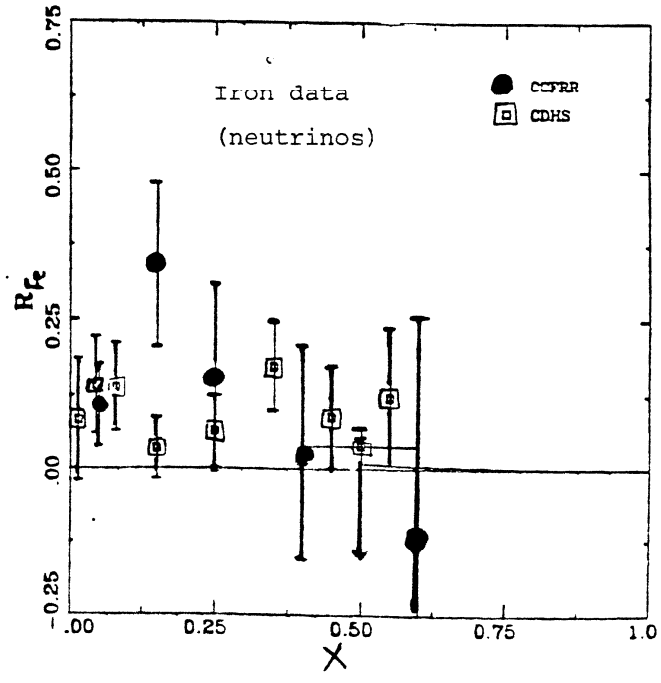

Figure 10. A comparison of narrow band neutrino data for R_{Fe} from CCFRR (Ref. 22) and CDHS (Ref. 10). The data are averaged over Q^2.

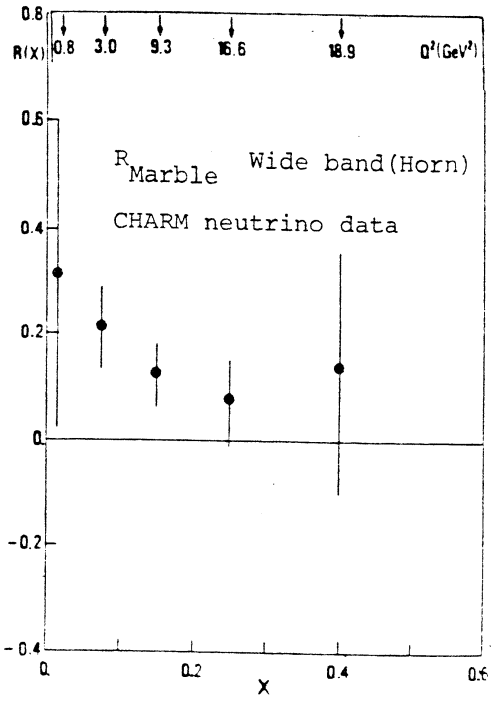

Figure 11. Values of R extracted from wide band horn neutrino data by the CHARM collaboration (Ref. 41). Systematic errors are estimated at ± 0.15. Only statistical errors are shown. The data are for bins of x averaged over Q^2.

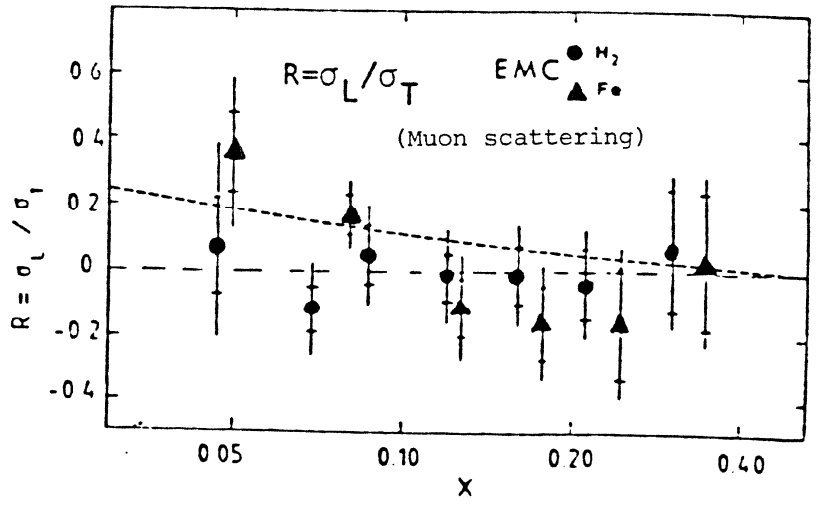

Figure 12. A comparison of R for hydrogen and iron from the EMC muon data (Ref. 42). Data have been averaged over Q^2. The dashed curve is the same QCD prediction shown in Figure 5.

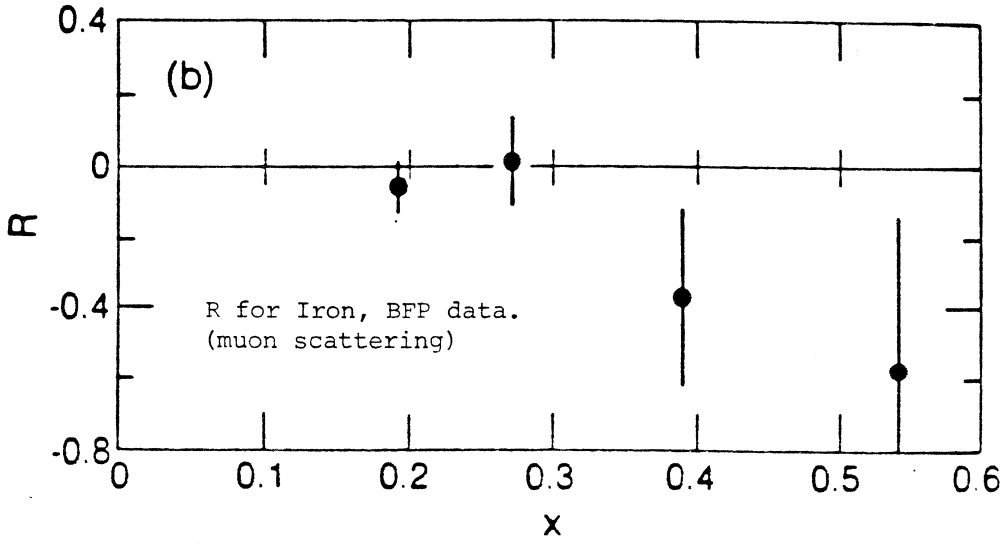

Figure 13. Data for R for iron from the BFP muon experiment (Ref. 43). Data have been averaged over Q^2 in bins of x. Only statistical errors are shown. The systematic errors are ± 0.11.

value $R_p = -0.01 \pm 0.11$. The mean value of R for iron is $R_{Fe} = 0.03 \pm 0.12$. Although these values of R are consistent with being equal, the large systematic errors preclude any investigation of a possible nuclear dependence of R. The EMC data for hydrogen and iron[42] averaged over Q^2 for fixed values of x are shown in Figure 12. The BFP collaboration has reported preliminary data on R for iron (no hydrogen data were taken). Their results (Meyers thesis[43]) are shown in Figure 13 and yield an average value $R_{Fe} = -0.06 \pm 0.06 \pm 0.11$.

It appears that the neutrino experiments obtain a value for R_{Fe} of 0.1 ± 0.1 and muon experiments obtain 0.0 ± 0.1. Differences between iron and hydrogen or deuterium of order 0.1 cannot be investigated. Although the results are all consistent with QCD predictions, given these large errors, they provide no stringent tests of QCD.

A first attempt at studying the possible nuclear dependence of R was performed by SLAC experiment E139 as a byproduct of a measurement of the ratio of structure functions of nuclei to those of deuterium.[8] Figure 14 shows the ratio of the cross sections σ_{Fe}/σ_d as a function of ϵ for E139 data as well as previous SLAC data. From Equation 17d, we see that the slope in such a plot is proportional to $R_{Fe} - R_d$. If R is independent of A the ratio σ_A/σ_d at a given x and Q^2 would be constant versus ϵ. Only at $x = 0.3$, 0.5, 0.7 and $Q^2 = 5$ $(GeV/c)^2$ are there E139 data at more than one value of ϵ. The slope of the best straight line fit to these data averaged over x, gives $d(\sigma_{Fe}/\sigma_d)/d\epsilon = 0.15 \pm 0.06$, which yields $R_{Fe} - R_d = 0.16 \pm 0.07$. As there is no evidence for a Q^2 dependence of the ratio σ_{Fe}/σ_d from E139, we include data at other Q^2 for comparison. The χ^2 for the lines with zero slope in Figure 14 is 35 for 14 degrees of freedom (E139 data only), whereas the χ^2 for the sloped lines is 16 for 13 degrees of freedom. The low Q^2 data of Stein et al[44] is also consistent with the sloped lines. This apparent difference between R_{Fe} and R_d could resolve the apparent discrepancy between the E139 and EMC cross section ratios at $x \leq 0.3$ shown in Figure 15. The ratios of F_2^{Fe}/F_2^d extracted from the cross sections at $\epsilon = 1$ are shown in Figure 16, which indicates a fair agreement between the two experiments, albeit

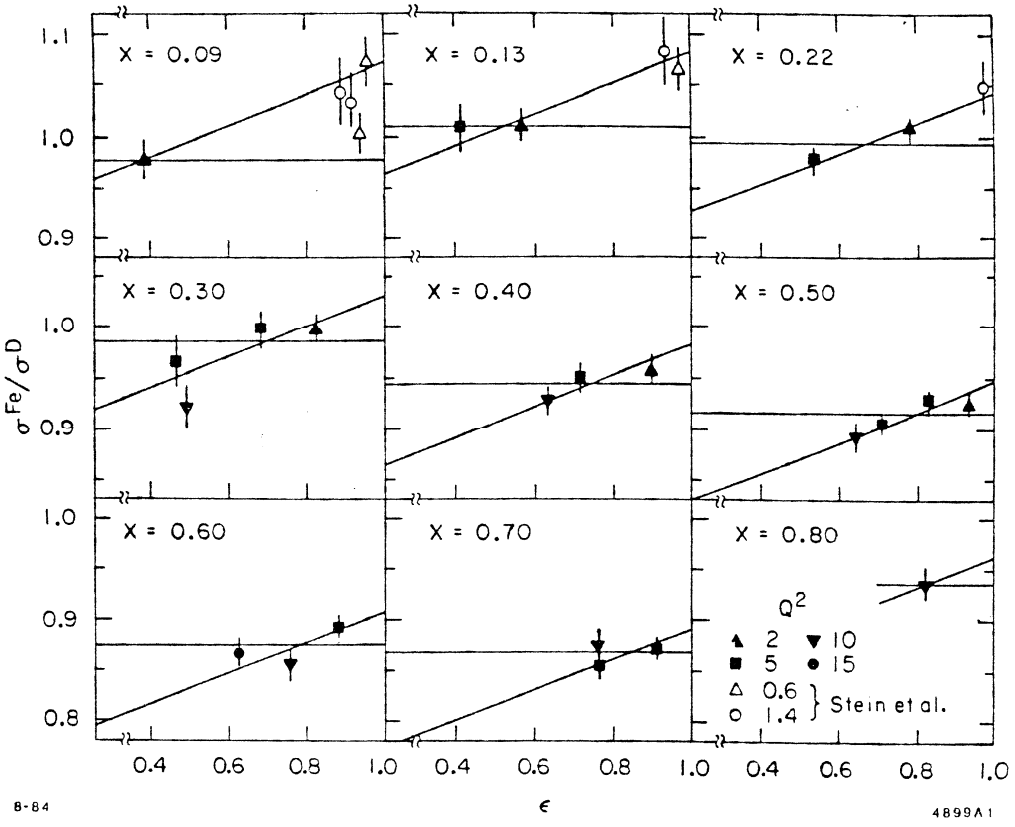

Figure 14. E139 results for σ_{Fe}/σ_d at various x and Q^2 values versus the virtual photon polarization parameter ϵ. The error bars are statistical only. Also shown are data from a Cu target from Stein et al (Ref. 44). The flat lines and the sloped lines were determined from fits to the E139 data at $Q^2 = 5.0\ (GeV/c)^2$ represented by the square symbols.

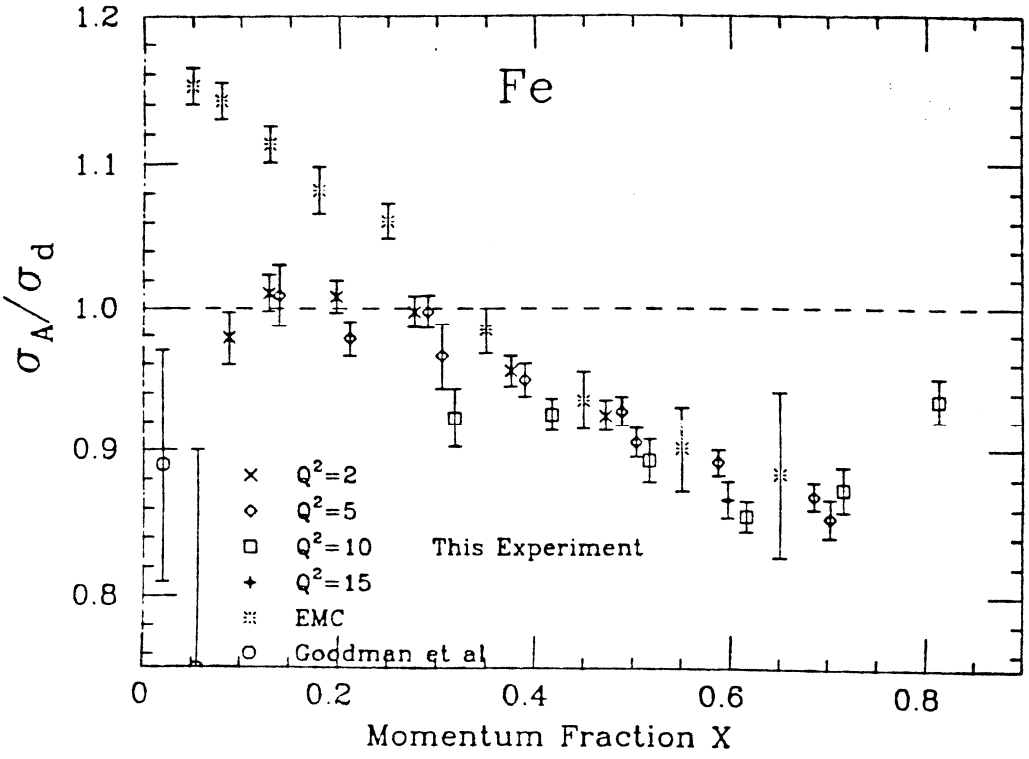

Figure 15. E139 results for σ_{Fe}/σ_d as a function of x for various values of Q^2, along with higher energy muon data from Refs. 7and 45.

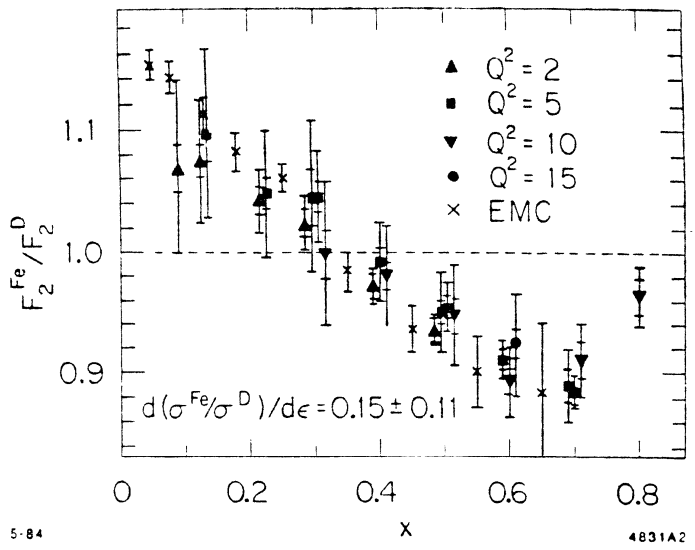

Figure 16. E139 results for the ratio of deep inelastic structure functions per nucleon F_2^{Fe}/F_2^d extracted at $\epsilon = 1$ from measurements of the cross section ratios σ_A/σ_d at various ϵ assuming the slope $d(\sigma_{Fe}/\sigma_d)/d\epsilon = 0.15 \pm 0.11$ is the same at all ϵ. The inner error bar is the statistical error while the outer bar indicates the additional systematic uncertainty from the extrapolation to $\epsilon = 1$. Also shown are the EMC data from Ref. 7.

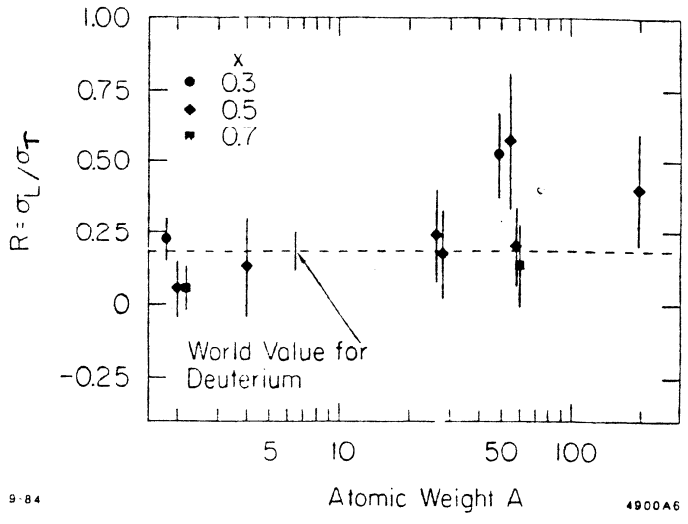

Figure 17. E139 results for $R = \sigma_L/\sigma_T$ at $Q^2 = 5$ $(GeV/c)^2$ and various x values versus nuclear weight A. The errors are statistical only. The average SLAC value and error for deuterium are also shown.

with large errors. Figure 17 shows the E139 results for R as a function of A at various x values at $Q^2 = 5\ (GeV/c)^2$ for d, ^{4}He, Al, Fe and Au. The trend of the data is for R to increase with A, but the errors are large. These results, while not *conclusive* on this point, suggest an A dependence of R which may be vital to understanding the EMC effect.

5. Motivation for a new R experiment

Of all the functions measured in deep inelastic lepton scattering, R is still one of the most poorly understood, despite numerous attempts to extract it from the cross sections. The quoted average values range from 0 to 0.5 with typical systematic errors of 0.1; even the two principal SLAC measurements disagree on the average value by a factor of 2. A weak kinematic variation with x and Q^2, which might give a partial explanation for these discrepancies, is suggested by the data but cannot be proved unambiguously because of large statistical and systematic errors in the individual measurements of $R(x, Q^2)$. Finally, recent indications of an A-dependence in R can only be taken as suggestive, not conclusive.

There are presently strong needs for more accurate data on R. In its own right, the kinematic variation of R with x and Q^2 provides an important test of QCD and an independent estimate of the strong coupling constant (see Equations 14 and 15). Accurate information on R is needed for studies of the structure functions measured in other experiments at SLAC, Fermilab and CERN. This is especially true when cross sections measured at widely different energies and angles – and from completely different experiments – are combined in a single global data set. Large errors in R will lead inevitably to large errors in the structure functions and in the conclusions that can be drawn about their kinematic variation. One of the principal remaining errors in studies of scaling violations, for example, comes from the large uncertainties in R. The recent indications of an A-dependence in R have thrown one more monkey wrench into these works, because most of the world data on inelastic muon and neutrino scattering have

been measured with iron targets. Accurate measurements of R for heavy nuclei are crucial to a better understanding of the EMC effect. Finally, it would be a relief to know, once and for all, just what is the true story about R.

Perhaps the major reason for all the uncertainties in R is the fact that this quantity has always been extracted as a byproduct of experiments designed to minimize the errors in other measured quantities. To date, nobody has performed an experiment explicitly designed to minimize the errors in R. We believe that such an experiment can now be done at SLAC, one that will reduce the systematic and statistical uncertainties in R by factors of at least 2 and 3 respectively. We are convinced that SLAC is the only place such an experiment can in fact be performed. This is part of the reason several physicists who do muon and neutrino experiments at CERN and Fermilab have joined this collaboration.

To make the best possible measurement of R, a precisely controlled, high intensity lepton beam whose flux is known to tenths of a percent is required. Also a very efficient detector that can be readily set at a wide range of scattered energies and angles to give the widest possible range of ϵ at each x, Q^2 point is necessary. That way one can measure the differential cross section with the exact same equipment at all angles and eliminate the normalization uncertainties that have plagued all previous measurements of R.

Such facilities are all readily available only at SLAC. Due largely to recent improvements in beam steering and monitoring, the electron beam in End Station A is known to a high level of precision. With the intense electron beams available here, 1% cross sections that would take days or months at other accelerators can be measured here in a matter of minutes or hours. The 8 GeV/c spectrometer is ideally suited to serve as the required detector of scattered electrons. With various modifications, this workhorse has been used in many experiments over the past two decades; its acceptance and other important properties are well understood at the present time. Moreover, this detector can be quickly moved to different scattered energies and angles with virtually no change in its optical

properties and no need for time-consuming surveys. Finally, intercomparisons between various target nuclei are a trivial matter at SLAC because of the interchangeable target system available in End Station A.

Equipment-related uncertainties can be so reduced in End Station A that the uncertainties in the radiative corrections loom as the largest remaining uncertainty in R. But here, too, we can do better than has been done previously. The radiative corrections in previous SLAC experiments[46] involved the "equivalent radiator" approximation to estimate internal bremsstrahlung and various peaking approximations to facilitate evaluation of the integral equations involved. Better methods using the more exact calculations of Tsai[48] and others[49] are now possible. In addition we now have large and fairly accurate global data sets of the cross sections over a wide kinematic range. These make a precise measurement of R feasible in a finite amount of running time by freeing us of the need to measure over large kinematic "triangles" at a single scattering angle. In contrast to the previous generations of SLAC experiments, we can measure only at the x, Q^2 kinematics desired. This has the added advantage that extensive interpolations are no longer necessary in the subsequent data analyses. Random errors in the individual $R(x, Q^2)$ will be truly independent, a feature that will make our experiment by far the best test of any kinematic variation in this quantity. Too often in the past, the individual $R(x, Q^2)$ represented a local average in this quantity because of these interpolations, and its random error was correlated with those of adjacent kinematic points.

This R experiment will measure simultaneously a number of quantities of current interest to the physics community:

- the average values of R_p and R_d (Are they 0, 0.15, or 0.30?).
- the kinematic variation of R_p and R_d with x and Q^2.
- the difference $R_d - R_p$ (and thus R_n) and its kinematic variation
- the differences $R_{Fe} - R_d$ and $R_{Au} - R_d$ and their kinematic variation.

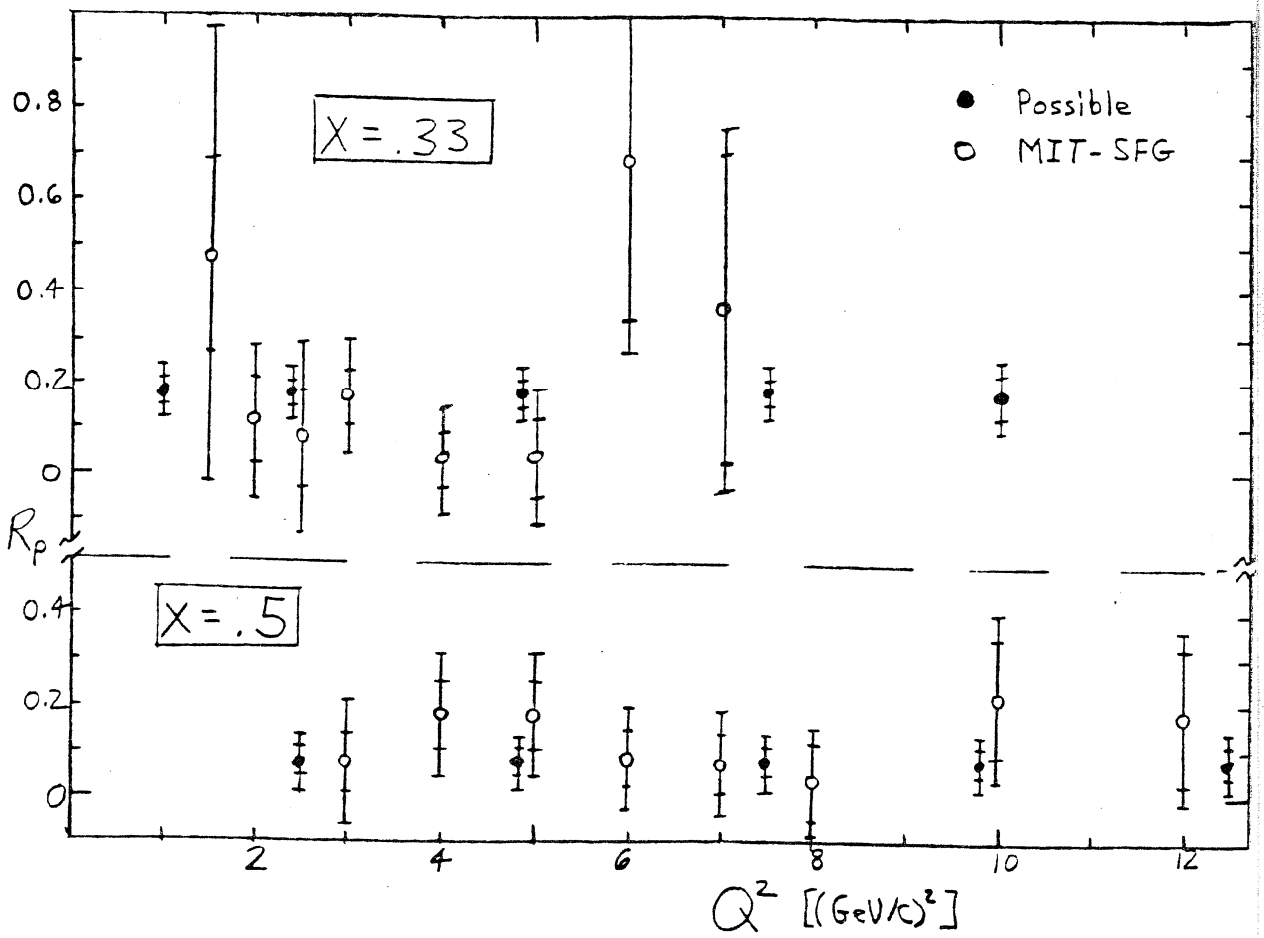

Figure 18. The MIT-SLAC data for R_p compared with possible data from this experiment at two values of x as a function of Q^2.

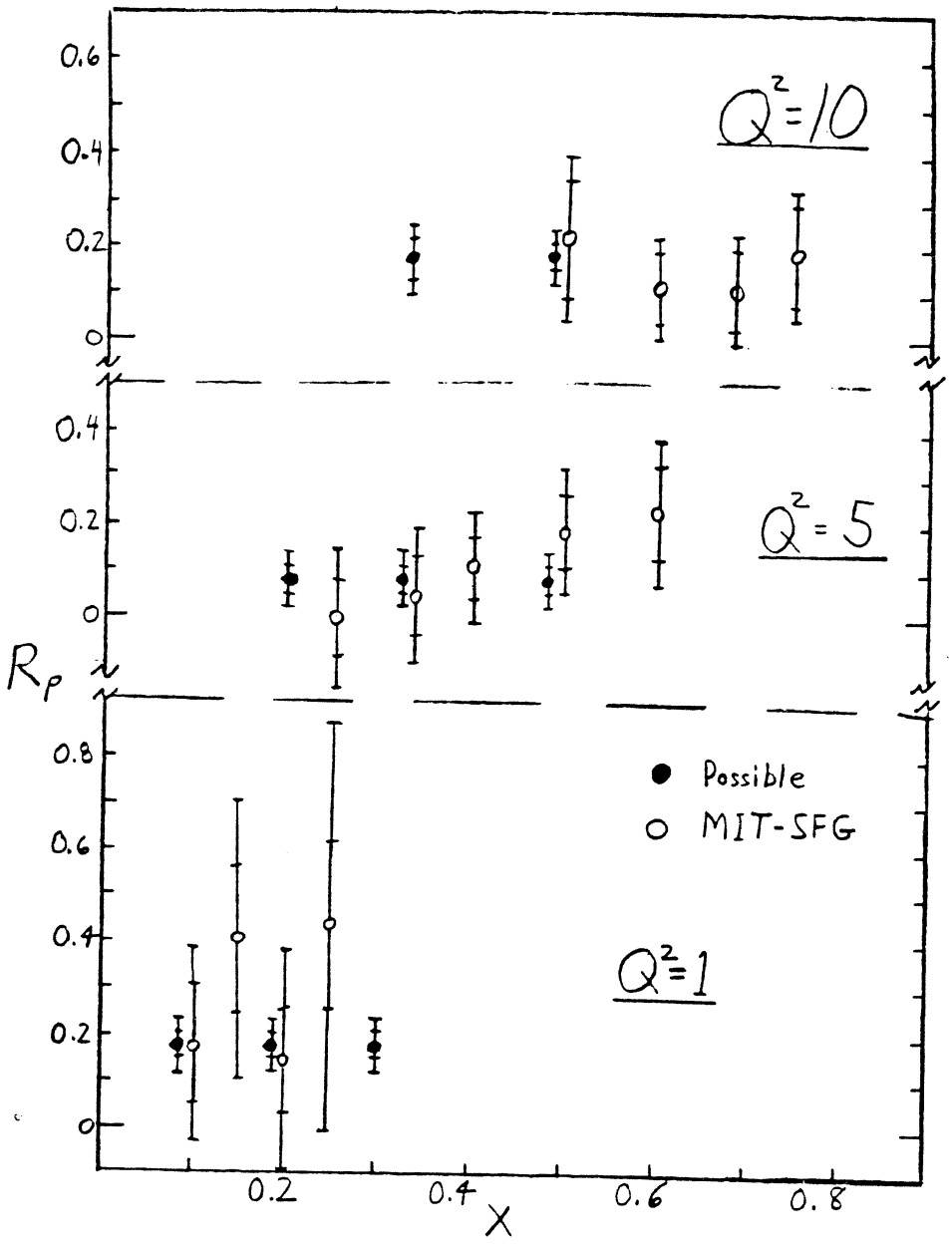

Figure 19. The MIT-SLAC data for R_p compared with possible data from this experiment at several values of Q^2 versus x.

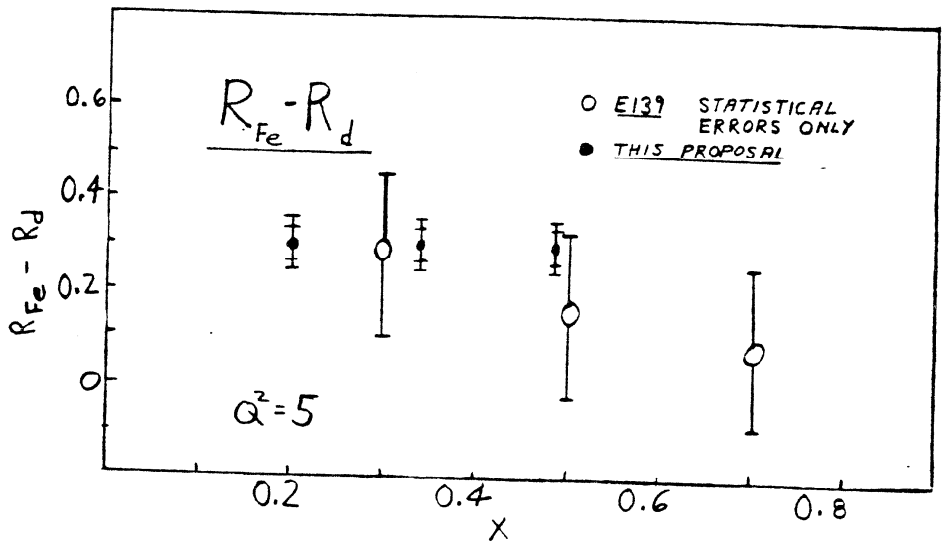

Figure 20. $R_{Fe} - R_d$ as a function of x for $Q^2 = 5$ $(GeV/c)^2$. The open circles are the E139 preliminary data (Ref. 3) with statistical errors only. The solid circles show possible data from this experiment. The inner error bars are the statistical errors and the outer are the systematic errors.

We can measure these quantities with much better accuracies than have been achieved previously, and help to resolve much of the great confusion that exists about them. Figures 18, 19 and 20 illustrate the precision of the data expected from this experiment compared with existing data. In this experiment we expect to reduce the systematic and statistical errors in R_p by factors of at least 2 and 3 respectively over previous experiments.

6. Apparatus

This experiment will use the 8 GeV/c Spectrometer and associated facilities in End Station A for the most part without modification. The only major change will be to improve two of the 8 GeV/c detectors. This Experiment will benefit from many improvements already made or planned for the ESA facilities.

6.1 Recent and planned improvements in End Station A

Since the last extensive measurements of R were made a decade ago at SLAC there have been many technical and methodological improvements in ESA. These will enable us to improve both the systematic and statistical accuracy of the results considerably.

Beam Monitors: The long term stability of the new toroid electronics is $\pm 0.1\%$. A new computer controlled calibration system soon to be installed will cross calibrate across all scales on a regular basis.

Target Density: The new generation of liquid targets, perfected in Experiments E136 and E139, have two fans circulating the liquid at high speed. With only one fan operating at 30% of capacity in E136 the density was measured to be independent of beam power to within the statistical accuracy of $\pm 0.5\%$. In the present experiment we should be able to determine the liquid target density to better than $\pm 0.25\%$.

Incident Beam Alignment: A set of wire SEM arrays are used to measure the beam position and intensity profile just upstream of the target on every pulse. The position information is used in a computer controlled system to adjust the beam steering between pulses. This system keeps the beam position stable to better then ± 0.05 cm. A second wire array further upstream will monitor the incident angle to within < 0.05 mr.

8 *GeV/c* Spectrometer: The End Station A power supply control system will soon be upgraded to a CAMAC based system. This will increase the reliability and ease of operation of the spectrometer. Fluctuations in momentum setting can be limited to $\pm 0.05\%$ by this system. Momentum changes will take only a few minutes.

The 8 *GeV/c* Detectors: The spectrometer is now equipped with 10 planes of wire proportional chambers in place of the old scintillator hodoscope system. Experience in Experiment E139 showed a tracking efficiency of $> 99\%$. In addition, the new chambers cover a factor of 2 larger momentum acceptance than the old hodoscopes. The existing poor resolution lead glass shower counter ($30\% /\sqrt{E}$ FWHM) will be replaced with a new high resolution lead glass shower counter ($8 - 10\% /\sqrt{E}$ FWHM). The existing single gas Cherenkov counter will be replaced by two gas Cerenkov counters to obtain higher pion rejection. These will be run in coincidence at low spectrometer momentum where the pion rate is high and they can be used at high pressure and efficiency. They will be run in OR mode at high spectrometer momentum where there are few pions. The additional gas Cerenkov counter and improved shower counter are expected to increase pion rejection by another factor of 300 over the factor of 5000 attainable with the old system. Thus our worst case pion/electron ratio of 200:1 will result in only a 0.02% pion contamination, which is more than a factor of 10 smaller than we can tollerate.

Acceptance of the Spectrometer: The momentum dependence of the spectrometer acceptance has been measured as part of Experiment E136 and will be

measured with greater accuracy again in this experiment. The proposed measurements of the spectrometer acceptance and matrix elements are described in detail in Section 8. As a result of these studies we will know the spectrometer acceptance to better than $\pm 0.5\%$ absolutely, and will determine any momentum dependence of the acceptance, which could affect determinations of R, to $\pm 0.2\%$ The momentum acceptance with the new detector package is a factor of two larger than for the E49b/E87 experiments.

6.2 OTHER APPARATUS

Beam: We will require operation of the accelerator with 1.6 μs pulse length at energies between 3 and 21 GeV with instantaneous currents ranging from 1 mA to the maximum obtainable through 0.4% full width slits. The NPI could be advantageously used in the low energy range.

Targets: The target assembly will include 20 cm long liquid hydrogen and deuterium targets, dummy cells, and 2.6% and 6% radiation length iron and 6% gold solid targets. This assembly will be similar to that used for E139.

Computers: The VAX 11/780 computer at ESA will handle data collection and on-line and off-line analysis. In addition, some radiative corrections programs may be run at Livermore. Some Monte Carlo studies will be done on the SLAC central computer complex.

7. Run plan

We plan to measure R over as wide a kinematic range as possible to test predictions of its x and Q^2 dependence. The low x region is particularly important for studying the A-dependence, since that is where existing measurements of the EMC effect disagree. High Q^2 data, although expensive in running time, are necessary for comparison with the theoretical predictions to help distinguish different contributions to R. The highest Q^2 data will be most relevant for comparison with CERN and Fermilab experiments.

We will measure R in the region of deep inelastic scattering readily accessible at SLAC (non-SLED) energies and with the 8 GeV/c spectrometer. Measurements will be made at about 14 kinematic points x, Q^2 in the region bounded by $0.1 \leq x \leq 0.5$ and $1.0 \leq Q^2 \leq 12.5$ $(GeV/c)^2$. That region overlaps much of the range covered in E139. The kinematic points are shown in Figure 20 and listed in Table III in Section 11. Fits to previous SLAC data were used to determine electron rates, and pion/electron and e^+/e^- ratios.

The settings of the experimental parameters have been determined by the following criteria:

Apparatus and Beam

1. The minimum angle of the spectrometer is 11.5 degrees.
2. The minimum momentum of the spectrometer is 1.0 GeV/c (to limit multiple scattering).
3. The maximum momentum of the spectrometer is 8 GeV/c (to avoid saturation of magnets causing a momentum dependence of the acceptance).
4. The NPI can be used for low energy running (to get increased beam current at some of the large angle points).
5. The maximum non-SLED beam energy is 21 GeV/c.

6. The available beam intensity versus beam energy is assumed to be the same as in Experiment E136, except when using the NPI.

7. The target length is 20 cm or less (so that the acceptance does not change with angle).

Rates and Backgrounds (set very conservatively)

8. The maximum usable trigger rate is about 0.1/pulse (to avoid large dead-time corrections).

9. The maximum allowed pion rate is about 1/pulse (to limit multiple tracks in the MWPCs).

10. The maximum allowed pion/electron ratio is about 200:1 (to avoid identification problems).

11. The maximum allowed e^+/e^- ratio is about 0.1 (to avoid large corrections and possible errors if the e^+ and e^- backgrounds are not equal).

Strategy

12. Measurements will be made at a minimum of three, typically five, and sometimes seven angles at each x, Q^2 point (to check for linearity in ϵ expected in Eq. 2).

13. Use the maximum range of ϵ obtainable at each x, Q^2 point consistent with acceptable counting rates and backgrounds (to reduce systematic errors which effect R as $\Delta R \sim \Delta\sigma/\Delta\epsilon$).

14. Measure a maximum of 40,000 counts per target per kinematic point.

The majority of running will be with hydrogen, deuterium and iron targets — with gold used to further check the A-dependence at selected values of x and Q^2. Any difference in R between deuterium and iron that is found online would call for more measurements with the gold target. The iron target of 2.6% radiation length matches the radiation length of the 20 cm deuterium target. The 6% radiation length iron target will be used at high Q^2 where the cross sections are

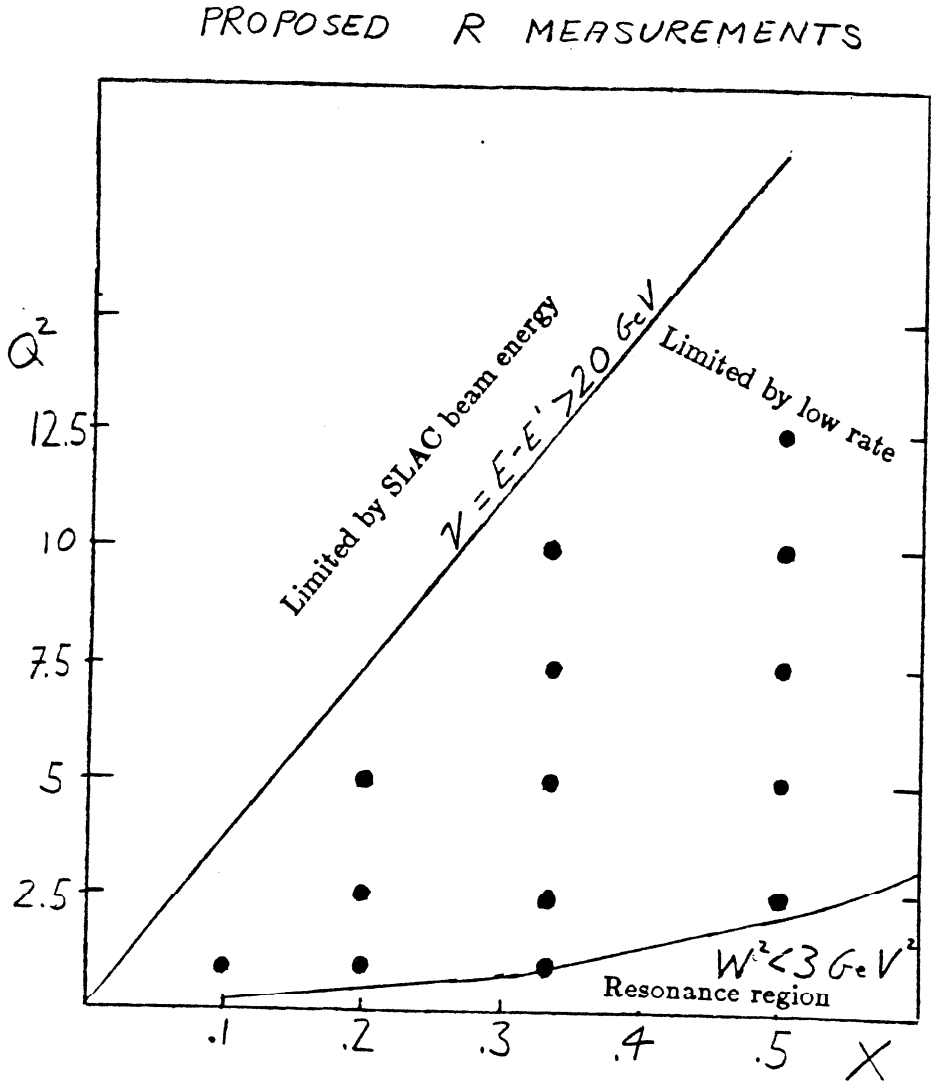

Figure 21. The x and Q^2 values of the proposed measurements of R. The kinematic limitations for a deep inelastic scattering experiment with high statistics using beam energy of 21 GeV and the 8 GeV/c spectrometer are shown.

low. At selected kinematic points both iron targets will be used as a test of radiative corrections.

The cross section will be measured at 3 to 7 different angles for each value of x and Q^2, and R can be extracted directly without interpolations. Many different incident energies will be required for the entire experiment. Since it is easier to change the angle and momentum of the spectrometer than the beam energy, we plan to take all the data at a particular energy (perhaps several x, Q^2 points) before moving to the next energy. Our experience is that energy changes of 1 *GeV* or less can be accomplished in an hour or two. If we run at 30 different energies between 3 and 21 *GeV*, these energy changes will consume about 50 hours.

The spectrometer angle can be changed within a few minutes and with a reproducible accuracy of better than ± 0.09 mr. Targets can be changed in less than 1 minute so that most systematic errors will cancel in the ratio of cross sections measured from different targets, as in E139. The ESA power supply control system will soon be upgraded to a fully CAMAC based system so the spectrometer momentum can be changed accurately and reliably in a few minutes. We generously allocate 10 hours for all the spectrometer changes.

Table III in Section 11 shows the actual data taking time for electron runs at each group of x, Q^2 points, assuming 100% efficiency at 180 pps (we assume 50% efficiency in our request for beam time). An additional time, averaging about 10% of the total, will be need for background runs on positrons. For dummy target subtraction for hydrogen and deuterium targets we will require an additional 2% running time. Table IV in Section 11 shows the total allocation of running time for this experiment, including all background measurements, calibrations, and overhead between runs.

8. Calibration efforts

The success of this experiment depends upon knowing the properties of the 8 GeV/c spectrometer with great precision. This instrument has been used in many previous experiments in which an accuracy of better than 1% was attained in measuring the ratio of one cross section to another. This experiment also measures ratios of cross sections. With the calibration runs outlined below we will be able to determine in several ways those properties of the spectrometer that can affect our results. These measurements are almost as important as the actual data taking and much care and time will go into them. We plan to measure:

1. the detailed acceptance of the spectrometer as a function of $\Delta\theta$, $\Delta\phi$ and $\Delta p/p$;
2. the variation of the acceptance with momentum and angular setting;
3. transport coefficients and their variation with spectrometer momentum;
4. the value of the spectrometer momentum setting relative to the electron beam.

The spectrometer transport coefficients will be remeasured without the beam using a floating wire technique. The other calibrations require beam time.

The following calibration procedures will be used:

Floating Wire Measurements: We plan to make floating wire measurements of the transport coefficients of the 8 GeV/c spectrometer. The emphasis will be on finding the momentum dependence of the transport coefficients. This procedure has the advantage of not using any beam time. A similar floating wire measurement of the 1.6 GeV/c spectrometer was done 10 years ago[46] in which the dominant coefficients were measured with an accuracy of better than 0.1% . The effects of the mass of the wire were also less than 0.1% . Improvements in technology in the past decade will more than compensate for the longer length of the 8 GeV/c spectrometer in the determination of the dominant coefficients.

If this technique proves to be accurate and convincing it may be possible to use less beam time on the elastic peak and jailbar calibration procedures.

Elastic Scattering: We will measure the position of the elastic peak in missing mass W^2 to determine: a) the precise incident beam momentum relative to the spectrometer setting, and b) the momentum dependence of the dominant transport coefficients. The center of the elastic peak can be located to better than 0.01 GeV^2. Depending on the exact kinematic conditions, this translates into an accuracy of better than 0.1% on the beam energy and spectrometer momentum. The momentum dependence of the spectrometer parameters can be tested by measuring the elastic peak at several different angles and momenta using the same incident beam. Again this will give an accuracy of about 0.1% on some combinations of the spectrometer transport coefficients. Experiment E136, currently being analyzed, has some information on this. Since the centroid of the elastic peak can be estimated to $\Delta W^2 = 0.003\ GeV^2$ with only 1000 counts, this work can be done in a few hours. Elastic cross sections also provide an ideal way to normalize data from this experiment to other SLAC $e-p$ experiments.

Running the Spectrometer at Zero Degrees: This will directly compare the spectrometer momentum and the A-bend calibration. This procedure was used during the 1967/1968 optics measurements of the spectrometer, where the emphasis was on measuring the transport coefficients. We will measure the momentum dependence of the spectrometer optics by measuring the location of central rays at different beam momenta. Using dark current from the accelerator, single events can be read directly by our detectors with a resolution of better than $\pm 0.04\%$ in $\Delta p/p$. It is also feasible to mount phosphoresent screens temporarily in the hut and run with small but measurable current if running with dark current is not satisfactory. These zero-degree tests can be done using low repetition rate test beam time.

Detailed Spectrometer Acceptance: Measurements of the spectrometer acceptance as a function of the reconstructed kinematic quantities $\Delta\theta$, $\Delta\phi$, and $\Delta p/p$

will be made with the different length targets used for this experiment. For these measurements the spectrometer will be set at an angle and momentum where the cross section is almost flat, and a series of high statistics runs will be taken where the data come in rapidly. The exact shape of the cross section will be measured by changing the spectrometer momentum and angle slightly and using the same part of the spectrometer for different kinematics. Six hours of dedicated runs combined with the regular data from the experiment will give a measure of the response function of the spectrometer-detector system with high statistical precision. Measurements taken during E139 indicate that for targets less than 20 cm long the acceptance varies less than 1% with the spectrometer angle out to 45 degrees.

Jailbar Method of Determining Transport Coefficients: This procededure was used for E89[37] and E136. A collimator consisting of vertical and horizontal bars will be placed in front of the spectrometer. The beam spot on a thin solid target and the center of the spaces between the bars determine a series of surveyed scattering angles. Data taken with the jailbars in place can be used to map out those angles and help determine various combinations of the spectrometer transport coefficients. To get $\pm 0.1\%$ accuracy in angle about 10,000 events are needed through each 1 cm jailbar hole. When this is done at several momentum settings about 8 hours of data taking will be required.

9. Radiative corrections

Radiative corrections to the measured cross sections will be performed using global fits to represent all previous SLAC electron scattering data as was done in experiments E89 and E139.

9.1 THEORETICAL APPROACHES

At present, several programs exist for the calculations of the radiative corrections. In general, the elastic and quasielastic tails are calculated in the "exact" Mo-Tsai[46] technique without resorting to the angle peaking approximation. There are several procedures to calculate the inelastic radiative corrections.

1. The approach using the equivalent radiator formalism and the angle peaking approximation as derived by Friedman and used by the MIT group[5] in SLAC experiments E49 and E87.

2. The Mo-Tsai technique[46] in the angle peaking approximation as coded by SLAC Group A and used in SLAC experiments E89[37,38] and E139.[3] This procedure was independently coded for muons by the Berekely-Fermilab-Princeton(BFP)[48] muon scattering experiment at Fermilab.

3. The "exact" Mo-Tsai technique without the angle peaking approximation as coded by the European Muon Collaboration (EMC).[47]

4. The Baldin procedure[49] which incorporates electroweak corrections and radiation from the quark lines in a parton model and was used by the BCDMS muon scattering experiment.[51] Similar procedures are incorporated in radiative corrections formalisms for charged current neutrino experiments.

9.2 ERRORS IN THE RADIATIVE CORRECTIONS

Errors in the radiative corrections could arise from:

(a) the approximations made in the theoretical model (eg. assuming only one hard photon is emitted),

(b) the approximations used to implement the model (eg. angle peaking aproximation),

(c) the cross sections used as input to the model for evaluating elastic, quasielastic and inelastic radiative tails.

Model Approximations: Tsai estimates[50] that his method is accurate to about 1% of the elastic and inelastic tails. This inaccuracy is due to neglecting contributions from radiation of two hard photons (order α^2). For the kinematics of this experiment, the inelastic tails are about 30% of the measured cross section, and the elastic and quasielastic tails are less than 10% . Thus neglecting the radiation of two hard photons could possibly cause a $< 0.5\%$ error in the radiatively corrected cross section.

Implementation of the Model: In the past, the peaking approximations used to implement the Mo-Tsai model have contributed an important uncertainty to the calculations of inelastic radiative tails.[3,5] This uncertainty can be essentially removed by using the "exact" calculations together with global fits to the structure functions, similar to the approach used in calculating elastic tails. Such an exact calculation requires more computer time, but need only be done for the 14 values in x, Q^2 to be measured in this experiment. This is the approach used by the EMC.[47]

Cross Sections: The radiative corrections method we will use requires *a priori* knowledge of the cross sections at kinematic points other than those measured in this experiment. The inelastic cross sections from hydrogen and deuterium have been carefully measured at SLAC energies at many kinematic conditions with a statistical accuracy of better than 2% . Preliminary results for the deuterium inelastic cross sections from E139 agree with a global fit to previous measurements to within the statistical errors of 1% . Experiment E139 also determined the ratio of cross sections for iron and gold to deuterium over the kinematic range of this proposal to 1% statistical accuracy. Quasielastic $e-d$ cross sections out to $Q^2 = 10\ (GeV/c)^2$ and $e-p$ elastic scattering out to $Q^2 = 32\ (GeV/c)^2$ have been measured recently with small errors in Experiments E133 and E136. We will take some elastic and inelastic data overlaping with those experiments; all this new cross section information will then be properly normalized between experiments and included in the global fits. This will substantially improve our

ability to calculate the elastic, quasielastic and deep inelastic radiative tails. We estimate there will be about a 1.5% uncertainty in the knowledge of the tails at our kinematic points due to uncertainties in the cross section at other kinematics. This will cause approximately a 0.5% systematic uncertainty in the radiatively corrected cross sections. The errors in the radiative corrections are expected to be largest at low x, low Q^2, and low ϵ, particularly the point at $x = 0.1$. The errors given here are average errors over our kinematic range.

9.3 CHECKS ON RADIATIVE CORRECTIONS

The error estimates given above for radiative corrections are supported by experimental and theoretical evidence:

1. The measurement of the electron scattering cross sections with different radiation length targets in order to check the corrections for external bremsstrahlung.[3]
2. Measurement of the photon spectrum from single photon bremmstrahlung by charged particles.[52]
3. Studies of two-photon effects and related processes.[54,55]
4. Comparison of theoretical models.

Comparison of Cross Sections from Different Thickness Targets: This tests sources of error a), b) and c) listed above, since the size of the inelastic tails increases with increasing radiation length. There are preliminary results from E139 on the ratio of the cross sections measured with 2% and 6% radiation length targets.[3] After averaging over carbon, aluminum and iron targets for $2 < Q^2 < 15\ (GeV/c)^2$ and $0.1 < x < 0.8$ the ratio $\sigma_{6\%}/\sigma_{2\%}$ is 1.001 ± 0.003. Aside from two anomalous points, the 40 individual ratios are consistent with random fluctuations about 1. within their 2% errors.

Photon Spectrum: The European Muon Collaboration has measured[52] the photon spectrum in bremsstrahlung processes in high energy scattering of muons

from hydrogen. They found agreement with the Mo-Tsai calculations and ruled out modifications suggested by Chahine.[58]

Two Photon Effects: These effects contribute sources of error a) and b) listed above. Studies of the elastic radiative tails between the elastic peak and inelastic threshold have been done at SLAC and in other electron scattering experiments. This tests the exact shape of the elastic tail where there are no other contributions.

In the deep inelastic region, one check on possible two photon exchange contributions is provided by a comparison of positive and negative electron and muon inelastic scattering. Such a comparison also provides a check on the contribution of hadronic radiation (which is included in the Baldin formalism[49] . A comparison of deep inelastic $e^+ - p$ and $e^- - p$ scattering done by the USCB group[54] yields $e^+ - p/e^- - p = 1.0027 \pm 0.0035$. An earlier measurement[55] at at SLAC found $e^+ - p/e^- - p = 1.001 \pm 0.008$. Similar measurments with muon scattering from nuclear targets are also consistent with unity.[56] A comparison of deep inelastic scattering of positive and negative muons on carbon at BNL[56] yields a ratio of 1.002 ± 0.017.

The BCDMS group[51] has used the comparison of positive and negative muon scattering on carbon to measure the interference structure function xG_3 and provide a test of the quark charges. In addition the total asymmetry which is zero at low Q^2 and increases to about 1% at $Q^2 = 100\ (GeV/c)^2$ results in a determination of the Weinberg angle ($0.23 \pm 0.07 \pm 0.04$). About half the observed asymmetry comes from radiative corrections as calculated using the Baldin formalism[49] and the other half comes from electroweak effects. One of the members of the BCDMS group (MV) is participating in this experiment. We plan to adapt the BCDMS radiative corrections programs to electron scattering and compare them to the program currently used at SLAC.

Another check on possible two-photon exchange contributions can be obtained from measurements of polarized electron scattering. A polarized target

asymmetry measurement of electron scattering in the resonance region[57] and elastic region[58] observed no asymmetry to within the experimental errors of 1.5% and 0.6% respectively.

All of the experimental checks for two photon effects in related processes described above are consistent with Tsai's estimate[50] of $\leq 1\%$ for the size of two hard photon radiation contributions.

In the comparison of R for iron and deuterium, one must estimate possible multiphoton effects on nuclear targets. Theoretical studies of such a possibility indicate[59] the such effects are small even for a very high Z material such as gold. Note also that the positive and negative muon comparisons were done on a carbon nuclear target both by the CERN BCDMS group[51] and the muon experiment[56] at BNL. A comparison of positive and negative muon scattering on an iron target was performed by the BFP muon experiment[42] at Fermilab. Their results are consistent with those of the BCDMS experiment and indicate that possible two photon exchange effects in iron are negligible.

Comparison of Models: Comparison of several radiative correction formalisms can be used to estimate the theoretical uncertainties in the procedures. Previous comparisons of radiative correction procedures were done by the MIT-SFG group.[2,5] In these studies the MIT procedure was compared to the Mo-Tsai procedure on the same set of data. There was an overall 3% normalization difference between the two procedures, plus a contribution that varied as $1/E'$. A normalization difference cannot affect the extraction of R, because R is a ratio of σ_L and σ_T, but the kinematic variation can. We plan to make a comparison of the Baldin and Mo-Tsai procedures. We will also modify the EMC procedure for muons, which uses the exact Mo-Tsai formalism, to handle electrons, and compare its results to those from the peaking approximation procedure.

9.4 IMPROVEMENTS ON RADIATIVE CORRECTIONS IN THIS EXPERIMENT

In this experiment we will check and improve upon the radiative corrections by:

1. Calculating the radiative effects using several different procedures.
2. Measuring the cross sections with different radiation length targets.
3. Measuring the cross sections at many values of ϵ to check for nonlinearity due to two-photon and other effects.
4. Adding more data from E133, E136 and E139 to the global fit.

In summary, we estimate that the error on the cross sections due to uncertainties in the radiative corrections will be less than 1% , and will be about equally due to uncertainties from lack of knowledge of the cross sections for calculating the radiative tails and from the approximation of single hard photon radiation. An uncertainty of 1% point-to-point in the cross sections translates into a systematic error of approximately 0.03 in R. For the A-dependence measurements $R_{Fe} - R_d$, some of the sources of error cancel, and we estimate a systematic error of 0.02 in the difference.

10. Experimental errors

Table V shows the uncertainty in the R measurements due to a variety of systematic errors. Items 1) to 6) have been explained in the Section 6.1 on improvements in ESA apparatus. In addition:

1. We will determine the background of electrons produced by mechanisms other than deep inelastic scattering by measuring the cross sections for the symmetrically produced e^+ (e.g. $\pi^0 \rightarrow \gamma\gamma \rightarrow e^+e^-$). These "positron" cross sections are measured by reversing the spectrometer polarity while holding all other variables fixed. We will only take data at kinematic conditions where the positron background is less than 10% , as estimated from a fit to

previous data measured in the same kinematic region. Since the symmetry of e^+,e^- production has been tested to the few percent level,[55] the error from this background results in a maximum error of a few tenths of a percent in our final cross sections.

2. We will take data with beam energy slits of 0.3 or 0.4% full width. Experience with the elastic peak position in many previous experiments indicates that the beam is on average centered within the slits.

3. Recent careful surveys have shown that the spectrometer angle can be set reproducibly to better than ± 0.005 degrees, or about ± 0.09 mr.

Summary of Errors

Absolute R: The combined systematic error in R due to instrumental uncertainty is ± 0.018. When this error is combined in quadrature with the radiative correction uncertainties, estimated in Section 9 to be ± 0.03, we get an estimated systematic error of ± 0.035. Note that compared to previous SLAC experiments, we are more cautious in our estimates of errors due to radiative corrections for $x > 0.2$.

The typical statistical error in R is ± 0.026. When combined in quadrature with the systematic error, this yields a total error of ± 0.043 in the absolute measurement of R. These errors compare favorably with existing systematic errors of typically ± 0.07 and statistical errors ranging from 0.07 to 0.15. These improved errors are illustrated in Figures 18 and 19 where they are compared to the MIT-SFG values.

Differences in R: In the measurement of the differences $R_d - R_p$, $R_{Fe} - R_d$ and $R_{Au} - R_d$, many systematic errors cancel because the data for different targets is taken under almost identical conditions. We estimate the combined systematic error in the measurement of the *difference* in R due to instrumental uncertainty to be ± 0.009. The systematic errors due to uncertainties in the radiative corrections is estimated to be ± 0.02. It is smaller than for the absolute

measurements because the corrections for different targets of the same radiation length at identical kinematic conditions are almost identical. The total systematic error in the difference measurements is ±0.022.

The statistical errors for the difference measurements are 1.4 times larger then for the absolute measurements because two targets must be used. When the systematic and statistical errors are combined in quadrature this yields a total error of ±0.043. Figure 20 shows the dramatic improvements possible in the quantity $R_{Fe} - R_d$ over what was obtained in Experiment E139.

The increased accuracies for this proposed experiment are possible because of improved equipment now available, the large existing data base for radiative corrections and better analysis techniques developed in over a decade of running at SLAC. Thus with an experiment dedicated exclusively to measuring R, we can reduce the systematic and statistical errors by factors of 2 and 3 respectively.

11. Request from the laboratory and proposed schedule

Beam conditions:

Energy:	3 to 21 GeV
Pulse width:	1.6 μsec
Slits:	0.4% full width
Current:	1 mA to maximum through 0.4% slits
Energy changes:	Frequent, about 30 in ≈ 0.5 GeV steps
	Time for energy changes: about 50 hours

Beam time at 180 pps 100% efficiency:

Full Linac	312 hours
Nuclear Physics Injector	24 hours

Total Time: With 50% effectiveness (including experimental and accelerator downtime and operation at less than 180 pps) we will use a total of 732 hours of accelerator time. This is 1 calendar month (not February).

Checkout: About 3 weeks at low repetiton rate, preferably non-SLED.

This experiment would benefit if the high powered SLC klystrons were installed in sectors 25 through 30 to increase the energy of the NPI beam. Any increase in the beam energy from the full linac up to the 24 GeV capacity of the A-bend would improve our experimental results in the high Q^2 region.

Target and Scattering Chamber: Standard End Station A target assembly with:

20 cm liquid hydrogen cell,

20 cm liquid deuterium cell,

20 cm dummy cell,

Assorted solid targets of iron and gold,

Al-ZnS solid target,

Distributed thin solid targets for jailbar work,

A no target position,

Scattering Chamber with targets visible from 11 to 46 degrees in the 8 GeV/c spectrometer.

Spectrometer: 8 GeV/c spectrometer, surveyed and equipped to detect electrons with:

10 planes of MWPCs	existing
2 Cerenkov counters	many parts existing
lead glass shower counter	to be provided by the collaboration

Electronics and Computers: The normal complement of fast logic for a single arm experiment similar to E139. Additional segmentation of the lead glass and a second Cerenkov counter will require a couple more ADC and TDC modules be added to the existing electronics in Counting House A. The VAX computer in the Counting House will do all the on-line analysis and most of the off-line analysis. The SLAC central computer complex will be used for Monte Carlo studies of the spectrometer.

Proposed Schedule: We could be ready for data taking either late in the Fall 1985 run cycle or early in the Spring 1986 cycle. That would allow time for completion of ongoing experiments that interfere with operation of the 8 GeV/c spectrometer (experiment NE4) and give time for the floating wire measurements before the data taking.

Table III

Proposed run plan. Column 8 lists the number of scattering angles at which measurements will be made for each x, Q^2 point. In column 9, $\Delta\epsilon$ is the maximum ϵ range co vered at a given x, Q^2 point, and column 10 is the statistical error on the absolute measurement of R. The running time in column 11 assumes 180 pps at 100% efficiency.

		Targets								
x	Q^2	H_2	D_2	Fe(2.6%)	Fe(6%)	Au	Angles	$\Delta\epsilon$	Stat Err	Hours
0.10	1.0	x	x	x			5	0.30	0.030	14
0.20	1.0	x	x	x	x	x	5	0.36	0.026	18
	2.5	x	x	x			5	0.37	0.026	12
	5.0	x	x	x			3	0.28	0.030	17
0.33	1.0	x	x	x	x	x	5	0.30	0.026	18
	2.5	x	x		x		7	0.42	0.026	8
	5.0	x	x		x	x	5	0.40	0.026	16
	7.5	x	x		x		5	0.40	0.026	25
	10.0	x	x		x		3	0.20	0.045	28
0.50	2.5	x	x	x	x	x	5	0.51	0.026	17
	5.0	x	x		x		3	0.40	0.026	18
	7.5	x	x		x		5	0.40	0.026	25
	10.0	x	x		x		5	0.40	0.030	28
	12.5	x	x				3	0.35	0.035	26

Total Hours = 270

TABLE IV

TIME ALLOCATION

	HOURS	COMMENTS
BEAM TIME		
Data taking	270	180 pps 100% efficiency
Dummy target	5	" "
Background (e+/e-)	27	" "
Calibration: Elastic	5	" "
Acceptance	6	" "
Jailbar	8	" "
Radiative Corrections data	15	" "
TOTAL BEAM TIME	336	@ 180 pps 100% efficiency
50% EFFICIENCY	336	downtime and rep rate loss
ENERGY CHANGES	50	30 changes of < 1 GeV
SPECTROMETER CHANGES	10	
TOTAL CALENDER TIME	732	30.5 days

TABLE V

SYSTEMATIC ERRORS

SOURCE	± UNCERTAINTY	± ERROR IN R	
		ABSOLUTE	$R_{Fe} - R_d$
INSTRUMENTAL			
1. Charge monitor fluctuations	0.1%	0.004	0.004
2. Spectrometer momentum setting	0.05%	0.003	0.003
3. Target density	0.25%	0.008	0.008
4. Incident beam alignment	0.05 mr	0.002	0.001
5. Acceptance (momentum dependence)	0.2%	0.007	-
6. Electron identification	<0.1%	<0.004	-
7. e+/e- background asymmetry	<0.2%	<0.007	-
8. Incident energy	0.1%	0.007	0.001
9. Spectrometer angle	0.09 mr	0.005	-
COMBINED INSTRUMENTAL ERRORS		<0.018	<0.009
RADIATIVE CORRECTIONS ERRORS	1%	0.03	0.02
TOTAL SYSTEMATIC ERRORS		0.035	0.022
TYPICAL STATISTICAL ERROR		0.026	0.037

APPENDIX A

Kinematics for muon and neutrino scattering

For high energy muon scattering experiments (neglecting terms of order M^2/Q^2 and M/E) the differential cross section given by Equation 1 is equivalent to:

$$\frac{d^2\sigma}{d\Omega dE'} = \frac{4\alpha^2}{Q^4}\frac{E'^2}{\nu}\cos^2(\theta/2)F_2(x,Q^2)\Big(\frac{1+\epsilon R(x,Q^2)}{1+R(x,Q^2)}\Big) \qquad (A.1)$$

$$\frac{d^2\sigma}{dxdy} = \frac{8\pi\alpha^2}{Q^4}MEF_2(x,Q^2)\Big(\frac{1-y}{\epsilon}\Big)\Big(\frac{1+\epsilon R(x,Q^2)}{1+R(x,Q^2)}\Big) \qquad (A.2)$$

where $y = \nu/E$ is the inelasticity. At large ν the virtual photon polarization ϵ can be represented by the expression:

$$\epsilon = \frac{2(1-y)}{1+(1-y)^2}. \qquad (A.3)$$

This function is shown in Figure A1. It illustrates the fact that small values of y correspond to $\epsilon = 1$ and large y coresponds to $\epsilon = 0$.

The extraction of R in neutrino scattering can be done using the sum of neutrino and antineutrino cross sections. The expression (in the limit of large ν and neglecting M^2/Q^2 and M/E terms) can be obtained by the substitution $8\pi\alpha^2/Q^4 \rightarrow G^2/\pi$, $F_2 \rightarrow F_2^{\nu,p}$ and $R \rightarrow R(\nu,\bar{\nu})$ in Equation A.2.

$$\frac{d^2(\sigma^\nu+\sigma^{\bar{\nu}})}{dxdy} = \frac{G^2ME}{\pi}F_2^{\nu,p}(x,Q^2)\Big(\frac{1-y}{\epsilon}\Big)\Big(\frac{1+\epsilon R(x,Q^2)}{1+R(x,Q^2)}\Big) \qquad (A.4)$$

Using Equation A3, this is equivalent to

$$\frac{d^2(\sigma^\nu+\sigma^{\bar{\nu}})}{dxdy} = \frac{G^2ME}{\pi}F_2^{\nu,p}(x,Q^2)\Big[1+(1-y)^2\Big]\Big[1+\epsilon(y)R(x,Q^2)\Big]. \qquad (A.5)$$

In analogy with electron scattering, R can be extracted from data at the same x and Q^2 taken at different incident neutrino energies and therefore at different

values of y. The systematic errors in such an analysis come from uncertainties in the normalization of the data taken with different energies, since the incident neutrino fluxes are not well known, and from resolution smearing effects.

Neutrino and antineutrino data can also be used to place limits on the value of R at large values of x. This procedure is best illustrated by rewriting the individual neutrino and antineutrino differential cross sections in terms of quark and antiquark distributions, again neglecting terms of order M^2/Q^2 and M/E (the exact expressions can be found in Reference 10):

$$\frac{d^2\sigma^{\nu,\bar{\nu}}}{dxdy} \simeq \frac{G^2 M E_\nu}{\pi}\left[(1-y)F_2^{\nu,\bar{\nu}} + \frac{y^2}{2}2xF_1^{\nu,\bar{\nu}} \pm (y-\frac{y^2}{2})xF_3^{\nu,\bar{\nu}}\right] \qquad (A.6)$$

$$2xF_1^{\nu,\bar{\nu}}(x,Q^2) \simeq q(x,Q^2) + \bar{q}(x,Q^2) \qquad (A.7a)$$

$$F_2^{\nu,\bar{\nu}}(x,Q^2) \simeq 2xF_1(x,Q^2) + F_2(x,Q^2) \qquad (A.7b)$$

$$xF_3^{\nu,\bar{\nu}}(x,Q^2) \simeq q(x,Q^2) - \bar{q}(x,Q^2) \pm 2x[s(x,Q^2) - c(x,Q^2)] \qquad (A.7c)$$

where

$$q = x(u + d + s + c) \qquad (A.8a)$$

$$\bar{q} = x(\bar{u} + \bar{d} + \bar{s} + \bar{c}) \qquad (A.8b)$$

and

$$\frac{d^2\sigma^{\nu}}{dxdy} = \frac{G^2 M E_\nu}{\pi}\left[q + x(s-c) + (1-y)^2[\bar{q} - x(\bar{s}-\bar{c})] + (1-y)F_L\right] \qquad (A.9a)$$

$$\frac{d^2\sigma^{\bar{\nu}}}{dxdy} = \frac{G^2 M E_\nu}{\pi}\left[\bar{q} + x(\bar{s}-\bar{c}) + (1-y)2[q - x(s-c)] + (1-y)F_L\right] \qquad (A.9b)$$

An upper limit on R^ν may be derived from Equation A.9, using the fact that $q(x)$, $s(x)$, and $c(x)$ are expected to be small at large x ($x > 0.4$). At large values

of x and y the upper limit is derived from the quantity $F_L^\nu/2xF_1^\nu$ where the upper limit on F_L^ν is obtained from the quantity,

$$\frac{d^2\sigma^\nu}{dxdy} - \frac{d^2\sigma^\nu}{dxdy}(1-y)^2 \leq F_L[(1-y)-(1-y)^2] + (\frac{M^2}{Q^2} \text{ terms}) \qquad (A.10)$$

and adding the contributions of the neglected M^2/Q^2 terms.[10] This technique only yields an upper limit because the antiquark and sea distributions are not exactly zero at large values of x.

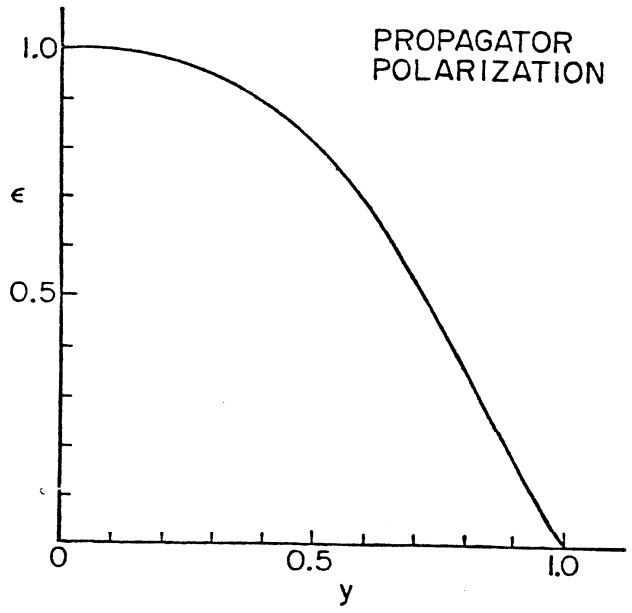

Figure A1: The virtual photon polarization as a function of the inelasticity $y = \nu / E$ (for large ν)

REFERENCES

1. G. Miller, Ph.D. Thesis, Stanford, 1970, SLAC Report No. 129(1972); G. Miller et al., Phys. Rev. **D5**, 528(1972)

2. E. M. RiordanPh.D. Thesis, MIT-LNS Report no C00-3069-176(1973), E.M. Riordan et al., Phys. Rev. Lett. **33**, 561(1974).

3. R. G. Arnold et al., Phys. Rev. Lett. **52**, 727(1984) and SLAC-PUB-3257(1983); R. G. Arnold et al. SLAC-PUB-3320(1984); S. Rock, SLAC-PUB-3420(1984), to be published in Proceedings of the Internation Conference on High Energy Physics, Leipzig, GDR, Jul y 1984; R. Arnold, SLAC-PUB-3434, to be published in the Proceedings of the 10th International Conference on Particles and Nuclei in Collision, Heidelberg, West Germany, July 1984.

4. J. J. Aubert et al., Phys. Lett. **105B**, 315 (1981); **114B**, 291 (1982).

5. A. Bodek et al., Phys. Rev. **D20**, 1471(1979).

6. H. E. Fisk and F. Sciulli, Ann. Rev. Nucl and Part. Sci. **32**, 499 (1982); G. Smadja, Proc. Int. Symp Leptons and Photons at High Energies, p. 444, W. Pfeil ed, Univ. Bonn., Germany, (1981).

7. J. J. Aubert et al., Phys. Lett. **123B**, 275(1983).

8. A. Bodek et al.,Phys. Rev. Lett. **50**, 1431; **51**, 534(1983).

9. A. Bodek, Rochester preprint UR-884(1984), Rapportuer's talk to be published in Proceedings of 'Neutrino 84' Dortmund, Germany, June 1984. This reference contains a discussion of recently completed and approved neutrino data runs for the CDHS(CERN WA1) and CCFR(Fermilab E616, E652 and E744) collaborations.

10. H. Abramowicz et al., Z. Phys. **C17**, 283(1983); **C15**, 19(1982).

11. C. G. Callan and D. G. Gross, Phys. Rev. **D22**, 156(1969).

12. R. P. Feynman, 'Photon-Hadron Interactions', W. A. Benjamin Inc. Reading, Mass. 1972.

13. R. Barbieri, J. Ellis, M. K. Gailard and G. G. Ross, Nucl. Phys. **B117**, 50(1976).

14. G. Altareli in 'New Phenomenon in Lepton-Hadron Physics', p. 215, Plenum Press, N.Y. 1980, D. E. C. Fries and J. Wess eds.

15. R. D. Field in 'Quantum Chromodynamics', p. 97, La Jolla, 1978, AIP Conference Proceedings No. 55, 1979.

16. A. De Rujula, H. Georgi, D. Politzer, Ann. Phys. **103**, 315(1977).

17. I. Hinchcliffe and C.H. Lewellyn Smith, Nucl. Phys. **B128**, 93(1977); G. Fox, Nucl. Phys. **B131**, 107(1977).

18. A. Buras et al., Nucl. Phys. **B131**, 308(1977); **B132**, 249(1978).

19. D.W. Duke et al., Phys. Rev. **D25**, 71(1982);A. Devoto et al. Phys.Rev. **D30**, 541(1984); Phys. Lett. **138B**, 418(1984); see also S. N. Coulson and R. E. Ecclestone, Nucl. Phys. **B211**, 317(1983).

20. L. F. Abbott and R. M. Barnett, Ann. Phys. **125**, 276 (1980).

21. A. Devoto, D. W. Duke, J. F. Owens and R. G. Roberts, Phys. Rev. **D27**, 508 (1979).

22. D. MacFarlane et al, Fermilab PUB-83/108-Exp(1983), to be published in Z. Phys. C, Oct. 1984, D. MacFarlane, Ph.D. Thesis, Caltech 1983 (available as Nevis preprint R1297); M. V. Purohit, Ph.D. Thesis, Caltech 1983 , (available as Nevis preprint R1298).

23. R. K. Ellis, W. Furmanski and R. Petronzio, Nucl. Phys. **B207**, 1,(1983); **B212**, 29(1983).

24. K. J. Kim, Phys. Lett. **76B**, 95(1978); For other references related to the influence on R from p_t effects see also: R. C. Hwa, S. Matsuda and R. G. Roberts, Phys. Lett. **76B**, 347(1978); see also H. Caprasse, Phys.

Rev. **D24**, 185(1983); T. Kobayashi, and N. Yamazi, Prog. Theo. Phys. **65**, 282(1981); S. Wada, Prog. Theo. Phys. **62**, 475(1979); T. Akiba, Prog. Theo. Phys. **67**, 1882(1982);D. Koniz, Z. Phys. **C18**, 63 (1983); M. Pennington, et al., Nucl. Phys. **B192**, 85 (1981).

25. I. Hinchcliffe, private communication.
26. M. Gluck and E. Reya, Nucl. Phys. **B145**, 24(1977).
27. C. Altarelli and G. Martinelli, Phys. Lett. **76B**, 89(1978).
28. A. Nakamura, G. Pancheri and Y. N. Srivastava, Z. Phys. **C21**, 243 (1984); P. K. Malhotra, R. Orava, Z. Phys. **C18**, 53 (1983).
29. L. F. Abbott, E. L. Berger, R. Blankenbecler and G. L. Kane, Phys. Let. **88B**, 157(1979).
30. L.F. Abbott,W. B. Atwood,R. M. Barnett, Phys. Rev. **D22**, 582(1980).
31. S. Fredriksson, M. M. Jandel, T. Larsson, Z. Phys. **C14**, 35(1982).
32. F. E. Close and R. G. Roberts, Z. Phys. **C8**, 57(1981).
33. F. Bobisut, to be published in Proceedings of the "Neutrino 84" Conference, Dortmund, Germany, June 1984.
34. H. Abramowicz et al, Z. Phys. **C25**, 29 (1984).
35. J. J. Aubert et al., Phys. Lett. **123B**, 123(1983).
36. F. J. Hasert, Fermilab Muon Proposal E665, T. B. W. Kirk and V. Eckhardt spokesmen.
37. M. D. Mestayer et al., Phys. Rev. **D27**, 285(1983).
38. M. D. Mestayer, Stanford Ph.D. Thesis, SLAC 214,1978.
39. B. A. Gordon, et al., Phys. Rev. **D20**, 2645 (1979).
40. J. J. Aubert, et al., Phys. Lett. **121B**, 87 (1983).
41. F. Bergsma, et al., Phys. Lett. **141B**, 129 (1984).

42. K. Rith, Review talk, published in Proceedings of the European Physical Society, Brighton, England (1983).

43. A. R. Clark, et al., Phys. Rev. Lett. **51**, 1826 (1983); P. D. Meyers, Ph.D. Thesis, Berkely, (1983), available as LBL-17108 (1983).

44. S Stein et al., Phys. Rev. **D12**, 1884(1975).

45. M. S. Goodman et al., Phys. Rev. Lett. **47**, 293(1981).

46. W. B. Atwood, Ph.D. Thesis, Stanford, 1975, SLAC Report No. 185 (1975).

47. J. J. Aubert et al., Phys. Lett. **121B**, 87(1983).

48. L. W. Mo and Y. S. Tsai, Rev. Mod. Phys. **41**, 205(1969); Y. S. Tsai, SLAC-PUB-848(1971), Lectures given at the NATO Advanced Institute on Electron Scattering and Nuclear Structure, Cagliani, Italy, 1970.

49. D. Y. Baldin et al., Yad. Phys. **29**, 499(1979), and Nucl. Phys. **B197**, 1(1982).

50. Y. S. Tsai, private communication, October 1984.

51. A. Argento et al., Phys. Lett. **120B**, 245(1983); A. Argento et al., Phys. Lett. **140B**, 142(1984).

52. J. J. Aubert et al., Z. Phys.**C22**, 341(1984).

53. C. Chahine, Phys. Rev. **D22**, 1062, 2727(1980); Phys. Rev. Lett. **47**, 1374(1981).

54. D. L. Fancher et al., Phys. Rev. Lett. **37**, 1323(1975).

55. L. S. Rochester et al., Phys. Rev. Lett. **36**, 1284(1976).

56. H. Jostlein et al., Phys. Lett. **52B**, 485(1974).

57. S. Rock et al., Phys. Rev. Lett. **24**, 748(1970).

58. T. Powell et al., Phys. Rev. Lett. **24**, 753(1970).

59. S.Brodsky and M. Soldate, SLAC, private communication, to be published, 1984.